ASSESSING THE USE OF ULTRASOUND TO QUANTIFY SPINE KINEMATICS

DANIEL A. DESROCHES

A THESIS SUBMITTED TO THE FACULTY OF GRADUATE STUDIES IN PARTIAL FULFILLMENT OF THE
REQUIREMENTS FOR THE DEGREE OF MASTER OF SCIENCE

GRADUATE PROGRAM IN KINESIOLOGY AND HEALTH SCIENCES
YORK UNIVERSITY
TORONTO, ONTARIO

July 2019

1 ABSTRACT

This thesis described the use of ultrasound in measuring multiplanar in-vivo lumbar spine motion in various positions of flexion and axial rotation using two separate ultrasound-based methods and was compared to surface-based optoelectronic motion capture. 14 instances of outlier range of motion were detected with the sagittal imaging method and complex movement sequences were uncovered with the transverse imaging method. Two error metrics were described and evaluated: (1) repeatability, which described the likeness of repeated images and subsequent image analysis; (2) robustness, which described the tolerance of the ultrasound measurement system to systematically induced error. The sagittal imaging method was considered robust and repeatable however the transverse method was less repeatable, with error potentially resulting from soft tissue creep. This thesis demonstrated that it is possible to measure multiplanar intervertebral motion via US and may help identify risky movement sequences which may appear normal in a surface-based motion capture investigation.

ACKNOWLEDGEMENTS

I would like to thank Dr. Janessa Drake for taking a chance on me, an Engineer with no formal Kinesiology background. Dr. Drake is a wonderful supervisor and I appreciate all her efforts in helping me design my thesis, write (more) coherently and maintain a high level of quality in all of my work.

I would like to acknowledge my colleagues Mario, Heather, Cecilia and Sam for their support, advice, and entertainment. A fun lab environment makes the long hours pass by just a little bit faster.

I would also like to thank my committee members Dr. Will Gage and Dr. Heather Edgell for their insightful questions and suggestions, both of which strengthened my final document. This thesis would not have been possible without Dr. Edgell's ultrasound machine and I am thankful that she entrusted me with it.

Last but not least, a big thank you goes to Scooter. I appreciate you and I am proud of you.

TABLE OF CONTENTS

LIST OF TABLES

LIST OF FIGURES

LIST OF ABBREVIATIONS

ASIS   Anteror Superior Illiac Spine

CI   Confidence Interval

EMG   Electromyography

ICC   Intraclass Correlation Coefficient

IMU   Inertial Measurement Unit

IPAQ   International Physical Activity Questionnaire

IRED   Infrared Emitting Diode

LBP   Low Back Pain

MMH   Manual Materials Handling

MRI   Magnetic Resonance Imaging

PSIS   Posterior Superior Illiac Spine

SP   Spinous Process

TP   Transverse Process

US   Ultrasound

2   INTRODUCTION

A systematic analysis of global burden of disease revealed that low back and neck pain is the leading cause of musculoskeletal disability world-wide (Vos et al., 2017) and will only worsen with an aging population. The likelihood of disabling low back pain (LBP) increases with age, and the Canadian population is aging. In 2016, for the first time in Census history, Canada had more seniors aged 65 and over than children under the age of 15. Further, in Ontario in 2017, LBP represented the largest number of claims (17%) (WSIB Ontario, 2017) and had a direct cost of $45.6 million. It has been estimated that direct costs typically account for one third of total costs whereas indirect costs (due to lost wages, lower productivity, retraining, etc.) account for the remaining two thirds (Katz, 2006). By this approximation, LBP cost Ontario approximately $136 million in 2017 alone. The astounding costs of LBP will only continue to grow with Canada's aging population and therefore, these facts suggest that more research is needed to understand spine function.

Spine biomechanics researchers can use invasive techniques or medical imaging to measure internal kinematics, or surface-based motion capture to measure external regional kinematics however each of these methods has its share of drawbacks. Current non-invasive in-vivo measurement technologies work well with flexion and extension motions, and significant in-vitro work has helped us understand related injury mechanisms. Despite abundant in-vitro research on axial rotation, associated in-vivo injury mechanisms remain less-well understood likely due in part to difficulty in quantifying kinematics. Ultrasound imaging may provide additional detail towards our understanding of in-vivo spine kinematics, which may reduce the risk work-related injuries, in activities of daily life, or as a result of aging.

Regional spine segments are commonly used to measure motion across a region such as the cervical, thoracic, and lumbar spine. To quantify kinematics in these regions, rigid bodies are placed at both ends of the region being quantified. For example, thoracic spine from T1 to T12, lumbar from L1 to

L5. Tracking regional spine segments using this approach has contributed significant knowledge of spine function (Ang et al., 2016; Frost et al., 2015; Schinkel-Ivy et al., 2015) but may not be ideal for measuring intervertebral axial rotation. In a bone pin study of internal/external rotation of the tibiofemoral joint, a rotation that is comparable in magnitude to lumbar axial rotation, the skin motion relative to underlying bone was enough to completely obscure the true motion of the knee joint (Benoit et al., 2006). Even though careful marker placement on the body can minimize error due to skin artifact (Cappozzo et al., 1996), there are few options for optimal marker placement on the lumbar spine. The measurement of lumbar axial rotation with surface-based motion capture remains problematic as a result. Regional segments track the cumulative intervertebral motion of all the joints within a region (i.e. lumbar flexion from L1 to L5) and so are not able to resolve differences in movement sequences at the intervertebral joint level (i.e. L1-L2 etc.). Unique intervertebral movement sequences have been documented in small samples of males in flexion/extension and axial rotation (Gatton and Pearcy, 1999; Gregersen and Lucas, 1967). While investigating axial rotation of the thoracic and lumbar spine during sitting, walking, and standing, Gregerson and Lucas (1967) found variations in rotation strategy among individuals. Specifically, some participants rotated predominantly at the T12 thoracolumbar junction, whereas others rotated more gradually from T1 through T7. Likewise, Gatton and Pearcy (1999) have shown that intervertebral movement sequences differ across individuals during voluntary flexion/extension, with some individuals initiating movement at different vertebral levels across tasks. Their findings related to movement variability were intriguing and provided key in insight into why some responses are associated with increased risk of injury, but these works received little follow-up due to the extensive resource demand and potential health risks in radiological investigations. It is for these reasons that alternate technology capable of capturing in-vivo intervertebral motion, especially axial rotation, was required.

Both invasive and non-invasive approaches for measuring internal spine kinematics have been explored. Invasive methods such as the surgical installation of intracortical bone pins (Gregersen and

Lucas, 1967; Lumsden and Morris, 1968; Lund et al., 2002; Rozumalski et al., 2008) have been used in select populations with limited tasks. Lund et al. (2002) documented cycles of flexion/extension, lateral bend and axial rotation via bone pins and optoelectronic motion capture in 34 low back pain pre-surgical patients. Using bone pins and an electromechanical transducer, both Gregersen and Lucas (1967) and Lumsden and Morris (1968) documented the in-vivo axial rotations of the thoracic and lumbar spine while walking and maximal range of motion (ROM) trials from standing and sitting in nine males. Rozumalski (2008) was the first to document the complex three-dimensional spine motion of four females and six males during gait with intracortical bone pins and optoelectronic motion capture. The kinematic data obtained from such studies are generally considered as a very precise and direct means of capturing skeletal motion relative to surface-based motion capture, but they require invasive surgery, tissue damage, and are difficult to justify especially in a healthy population.

Medical imaging methodologies such as magnetic resonance imaging (MRI) (Fazey et al., 2006) and videofluoroscopy (Cholewicki and McGill, 1992) are much less invasive and have been used successfully to examine internal kinematics. Cholewicki and McGill (1992) used videofluoroscopy to directly quantify the intervertebral joint flexion/extension across different sets of three vertebrae (limited by videofluoroscope field of view) and deformation of the lumbar spine ligaments in four participants during maximal effort deadlifts. Fazey et al. (2006) used MRI to track the migration of the nucleus pulposus at L1-L2 and L4-L5 in three asymptomatic participants as a proxy for the distribution of disc loading in positions of flexion/extension and/or rotation. They found consistent migration of nuclear material following sagittal plane motion but less consistent migration during rotation. The findings of Cholewicki and McGill (1992) and Fazey et al. (2006) contributed important details that helped advance our understanding of mechanics and injury mechanisms. However, medical imaging is restricted to static postures or quasi-static tasks (or quasi-static joints during a dynamic task) and cannot be used during dynamic tasks such as swinging a golf club or manual materials handling tasks, or tasks that require foot

movement (i.e. include gait) with the exception to videofluoroscopy. Videofluoroscopy can be used during such tasks, however it is restricted to one plane of motion, a limited field of view, and is also radiotoxic. Regardless of these limitations, these internal kinematic studies have contributed fundamental knowledge related to movement and mechanisms of injury to the field of spine biomechanics, but the methods have clear drawbacks which prevent their use in healthy populations or during functional movements. More investigation of intervertebral kinematics is needed.

There is demand for a tool capable of measuring three-dimensional intervertebral kinematics in a wide variety of environments and tasks. Ultrasound is a non-invasive and highly portable technology that has been used to analyze predominantly soft tissues within the body for over 20 years with usage ranging from detecting various tendon and ligament pathologies (Hodgson et al., 2012) to measuring the thickness and pennation angle of thoracic erector spinae musculature (Nairn, 2017). This technology has been applied to spine kinematics only recently, but the literature appears promising (Chleboun et al., 2012; Mayberry, 2017; McKinnon and Callaghan, 2019). Chleboun et al. (2012) found that ultrasound and MRI were similar in their ability to measure spinous process (SP) spacing in positions of flexion and extension. Likewise, Mayberry (2017) found no difference between ultrasound and MRI when measuring intervertebral lumbar axial rotation. These recent studies are encouraging, but the ability to measure multiplanar motion has not been evaluated and the associated error is yet to be assessed.

2.1 Thesis Scope

This thesis explores the ability to measure combined flexion and axial rotation motions via ultrasound coupled with optoelectronic motion capture. This research will first experimentally investigate an imaging acquisition window which was theoretically based on in-vivo anatomical measurements of lumbar vertebrae (Aylott et al., 2012; Kawchuk et al., 2011). Images may be captured and accurately analyzed within this theorized window. Then, the robustness and repeatability of the method will be assessed via induced error and analyses of ideal image repeats, respectively. Ideal images are objectively

assessed to offer the clearest anatomical landmarks for subsequent measurement and are found by iteratively scanning the area of interest. Lastly, this research will compare the kinematics quantified using external regional motion capture of the lumbar spine to kinematics measured by ultrasound during several simulated manual materials handling (MMH) tasks to stimulate spine flexion, axial rotation, or both combined. Pilot work on five participants (three females and two males) was the basis for the numeric data included in the hypotheses listed below.

2.2 Objectives

1. Quantify the **repeatability** of ultrasound measurements in neutral, flexion, and rotation postures (via comparison of ideal image repeats).
2. Quantify the **robustness** (i.e. tolerance of the method to induced error) of sagittal ultrasound measurements in neutral and flexion positions (via comparison of ideal and non-ideal measurements).
3. Quantify the **transverse orientation acquisition window** by tilting at L1.
4. Quantify the **sagittal plane acquisition window** by tilting at L1-L2.
5. Quantify **intervertebral motions** (flexion and/or axial rotation) during MMH tasks.

2.3 Hypotheses

1. **Repeatability**
    a. There will be a difference in ideal images within participants, within positions measured via SP spacing (i.e. not repeatable).
    b. There will be a difference in ideal image axial rotation measurements within participants, within positions (i.e. not repeatable).
2. **Robustness**
    a. There will be a difference between SP spacing measurements taken from ideal and non-ideal images (i.e. not robust).
3. **Transverse orientation acquisition window:** on average, transverse images will tolerate a 20° tilt or less, bidirectionally about the mediolateral axis.
4. **Sagittal plane acquisition window:** on average, sagittal images will tolerate a 14° tilt or less, bidirectionally about the longitudinal axis.

5. **Accuracy of intervertebral motion**

   a. Ultrasound will not identify additional outlier ROM when compared to surface-based regional motion capture.

   b. There will be a difference in axial rotation calculated by ultrasound compared to regional motion capture.

3 LITERATURE REVIEW

3.1 In-vitro

In-vitro research using both human and animal specimens has helped to document loading responses, mechanisms of injury, and the intricate mechanical behaviour of the lumbar spine. (Adams, 1995; Callaghan and McGill, 2001; Drake et al., 2008, 2005; Panjabi et al., 1982). In vitro methods have improved our understanding of some of the key intervertebral mechanics that may not have otherwise been identified. Some of these key findings include: In 1982, Panjabi et al. analyzed the ligament strain on cadaveric functional spinal units in order to describe the ligamentous contributions at end ranges of rotation, flexion, and extension. In 1995, Adams described complex behaviour of in-vitro specimens under load including non-linear stiffness, where a specimen becomes increasingly stiff as strain increases and viscoelasticity, where stiffness increases proportional to the loading rate. Callaghan and McGill (2001) determined that moderate compressive load combined with repetitive flexion-extension motion led to failure of porcine cervical spine segments (C3-C4) from intervertebral disc herniation not vertebral fracture. In 2005, Drake et al. uncovered accelerated failure in loading protocols involving combined axial rotation and compression and in 2008 demonstrated a postural dependence for facet joint interactions. These related intervertebral kinematic intricacies are difficult to observe in-vivo when using external motion capture, and so in-vivo intervertebral kinematics are poorly understood. Likewise, understanding intervertebral motion in-vivo is the main motivation for using internal motion capture methods such as radiography, magnetic resonance imaging (MRI) and in the case of this thesis, ultrasound imaging.

3.2 External Motion Capture

External marker-based motion capture methods, which include optoelectronic motion capture (with actively emitting LEDs or passively reflecting markers) and inertial measurement units, are best-suited to measure relatively large-scale movements over regions of the spine. Smaller movements such as non-sagittal motion at the tibiofemoral joint (Benoit et al., 2006), or motion measured near joint

centres of the greater trochanter or lateral malleolus are highly affected by skin motion relative to bone (Cappozzo et al., 1996). Rotations of 5° or less are commonly observed in lumbar axial rotation and therefore it is suspected that these small motions of the SPs would be similarly impacted by skin artifact. Skin artifact in the lumbar region is difficult to quantify due to limited space for installing both bone pins and surface markers onto the SP. Direct comparison between bone pins and surface markers is made even more difficult due to an 'anchoring' effect created by the bone pins on surrounding skin which disrupts the normal motion of surface-based markers (Westblad et al., 2002). For more information on research related to bone pins, see section 3.3.1. Primarily due to space limitations, lumbar region spine motion is typically measured across regions consisting of groups of two to five vertebral joints (Drake et al., 2006; Frigo et al., 2003; Gregory and Callaghan, 2008; McGill et al., 2015; Schinkel-Ivy et al., 2014). Interpretation of regional data typically assumes that all motion is evenly distributed across intervertebral joints or that it conforms to population average joint ranges of motion (ROM). However, several studies have not supported this assumption (Ochia et al., 2006; Pearcy et al., 1984; Yamamoto et al., 1989). Using biplanar radiography, Pearcy et al. (1984) showed that in-vivo flexion ROM was between 8° at L1-L2 to 13° at L4-L5. Similarly, Yamamoto et al. (1989) applied pure moments of 10 N-m on human cadaveric ligamentous lumbar spines (including the sacrum) to investigate three-dimensional ROM and found lumbar flexion ROM to be between 5.8° at L1-L2 and 10.0° at L5-S1. More recently, Ochia et al. (2006) used computed tomography (CT) scans to investigate three-dimensional spine ROM in-vivo and determined axial rotation was greater at L1-L2 than at L3-L4, and frontal plane translations were over 5mm at L1-L2 gradually decreasing across inferior levels.

In addition to differences in amount of ROM per joint, different movement strategies have been found within movements and within individuals for a given flexion/extension task (Gatton and Pearcy, 1999). Specifically, in their study on seven males and seven females, Gatton and Pearcy (1999), showed that the conventionally assumed 'top down' approach to flexion (i.e. movement initiated sequentially

from L1-L2 though L5-S1) was displayed in only 9% of the trials and upon repeating a task, some participants used a different sequence. Due to relative motion between skin and overlying markers, variable movement across intervertebral joints, and variable movement strategies within participants, current external marker-based motion capture technologies used to quantify regional spine kinematics may not be sufficient to capture the level of detail needed to understand the factors involved in influencing particular movement strategies and their associated risks/benefits.

3.3 Internal Motion Capture

Two groups of methods used in research allow the internal workings of the body to be viewed and/or quantified: intracortical bone pins and medical imaging. These tools have been applied successfully to the study of spine kinematics, but most are not suitable for routine use due to associated risks.

3.3.1 Bone Pins

Intracortical bone pins have been used to directly measure in-vitro and in-vivo three dimensional spine kinematics (Gregersen and Lucas, 1967; Lumsden and Morris, 1968; Lund et al., 2002; Rozumalski et al., 2008; Sahni et al., 1999) with high accuracy (Sahni et al., 1999), but are also invasive and surgical installation is difficult to justify especially in healthy populations. Justification for using healthy individuals is challenging due to the risk of infection or other complications (Stinton, 2011) and low sample size is typical (Gregersen and Lucas, 1967; Lumsden and Morris, 1968; Rozumalski et al., 2008). The requirement for a surgeon and medical facility is yet another burden to overcome in such studies. Gregersen and Lucas (1967) were the first to document in-vivo axial rotation of the thoracolumbar spine in seven unaffected males via bone pins during sitting, standing, and walking. Their work documented variation in both movement strategies and rotation ROM across participants, with one participant demonstrating significant rotation at the level of T12 (9°), and another demonstrating minimal rotation (3°) during gait (Gregersen and Lucas, 1967). Lumsden and Morris (1968) studied 10 unaffected males and found approximately 6° of maximal axial rotation at the L5-S1 joint while standing and sitting. In patients with

LBP, Lund et al. (2002) studied three-dimensional motion of the lumbar spine in chronic low back pain patients and discovered asymmetries in lateral bending, strongly coupled axial rotation during lateral bending, and significantly reduced flexion ROM compared to previously published normal population data. As in the case of Lund et al. (2002), recruited patients are often pre-surgical and therefore unlikely to be representative of an unaffected population. Therefore, despite the highly accurate three-dimensional internal kinematics offered by bone pins, the invasive surgical procedures, related risks, and requirement for suitable medical resources are often difficult to justify in a large sample of patients and/or unaffected individuals.

3.3.2 Medical Imaging

Medical imaging technologies such as those that are radiography-based (X-ray, videofluoroscopy and CT) and MRI have been used to generate valuable information about the human spine regarding physiological ROM (Pearcy et al., 1984) and architecture of both bone (Aylott et al., 2012; Panjabi et al., 1991) and muscle (Nairn, 2017). Pearcy and Tibrewal (1984) used bi-planar radiography to capture a frontal and sagittal plane image of the lumbar vertebrae in positions of maximal axial rotation and lateral bend. While X-ray produces high quality imaging of bone and has provided some fundamental information regarding the structure and function of the spine, this approach requires costly technology, is radiotoxic, is restricted to static postures and only produces two-dimensional images. Unlike X-rays, videofluoroscopy does not require static postures during imaging as it uses lower resolution X-ray to assemble a video of bone motion. Cholewicki and McGill (1992) were the first to report in-vivo measurement of spinal ligament elongation in Canadian powerlifters using videofluoroscopy (1992). Despite also having a reduced resolution of a collapsed 3D to 2D image and constrained field of view of, videofluoroscopy is considered an improvement over standard X-ray when studying dynamic tasks, but it is costly to acquire, access is limited to few hospitals is also radiotoxic. MRI, which is based on the response of hydrogen protons within bodily tissues to magnetism, can also be used to investigate spine kinematics. MRI is not

radiotoxic but is costly, difficult to access, and restricted to static postures due to the duration of the relaxation time (RT) of the sequence. The bore size is typically small which limits testing positions for participants, and the field of view remains restricted to the region of the radiofrequency coils. MRI has been used to quantify the changes in intervertebral foramen cross-sectional area in neutral and axially rotated positions (Mayberry, 2015), contributing to our understanding of nerve impingement risk during axial rotation. MRI has also been used to investigate in-vitro facet joint spacing during various combined motions, improving our understanding of the coupling between flexion and rotation motions (Drake et al., 2008). Although these methods have contributed fundamentally to our understanding of nerve impingements and the complex mechanical interactions within the spine, these technologies are not ideal for measuring three-dimensional spine kinematics due to physical constraints within the bore, the expenses of owning and operating the equipment (including the cost of an MRI technician), and the requirement of static supine-based postures.

In recent years, ultrasound technology has improved in its ability to view smaller and deeper targets, and has since been compared with several measurement methods ranging from MRI to digital cameras to determine ultrasound's viability as a kinematic measurement tool. A study in 2012 compared ultrasound to MRI in its ability to measure relative changes between vertebrae in various degrees of flexion and extension using one or two digitized points. Both MRI and ultrasound analyses showed strong interclass correlations (0.98 and 0.94) suggesting both are reliable measurement tools for this purpose (Chleboun et al., 2012). When measuring in-vitro osteoligamentous lumbosacral motion, ultrasound demonstrated good agreement and low absolute error as compared to digital photography using various anatomical points and digitization methods (van den Hoorn et al., 2016). Mckinnon & Callaghan (2019) used in-vitro methods to compare measures of intervertebral rotations via ultrasound (Sonosite M-Turbo) to optical motion capture (Optotrak, Certus) directly mounted to vertebral bodies. They found a correlation of greater than 0.90 for three different sagittal plane postures (flexion, neutral and extension)

suggesting sagittal plane posture had little effect on the ability to measure axial rotation and showed an average error of 0.1° or less between systems (McKinnon and Callaghan, 2019). Ultrasound has also been validated against MRI measures of vertebral axial rotation in human lumbar spines and no significant difference was found between the two methods (Mayberry, 2017). Therefore, there is direct evidence for the use of ultrasound in measuring single planes of intervertebral motion and the potential for measuring multiplanar intervertebral motion in-vivo.

3.3.3 Knowledge Gaps

The capability of measuring lumbar flexion/extension and axial rotation motions separately with ultrasound has been adequately demonstrated (Mayberry, 2017; McKinnon and Callaghan, 2019; van den Hoorn et al., 2016). What remained to be understood was the feasibility of tracking three-dimensional motion using ultrasound (i.e. simultaneously measuring flexion/extension along with axial rotation) and the related potential sources of error involved in doing so. Relevant error metrics that were employed to assess feasibility were repeatability (defined as the consistency of ideal image repeated measurements) and robustness (defined as the tolerance of the method to induced error). Therefore, the goal of this thesis was to investigate the ability to measure multiplanar intervertebral kinematics, reveal outlier ROM, investigate movement sequences and to assess the reliability and robustness of the system with the overall goal of improving our understanding of spine function or response to exposures.

4   METHODS

4.1 Overview

To assess error, sagittal and transverse ultrasound images were taken at the level of L1-L2 with the participant laying prone and supported in various postures. Ideal images were found by sweeping the transducer over the area of interest in an iterative fashion until the clearest echoes from required landmarks were obtained. Repeatability was assessed by comparing sequentially captured ideal images. Robustness was assessed by tilting and translating the ultrasound transducer systematically away from ideal images in four different directions, inducing potential error into the ideal images. This process generated ideal and non-ideal image pairs which served as the basis for the robustness assessment. An ideal image was one that contained distinct echoes whereas a non-ideal contained diffuse echoes but was still measurable. Optoelectronic motion capture recorded the motion of the ultrasound transducer, which was used to generate an ultrasound image acquisition window (i.e., orientation of transducer where images can be obtained with little expected error). In the second phase of the study, MMH tasks, participants completed reaching tasks while their pelvis was fixed to encourage motion about the spine. These movements were collected with both surface-based optoelectronic motion capture (between T10-S1) and ultrasound imaging. Sagittal and transverse plane ultrasound images were captured during these tasks at each vertebral level from L1 through S1 in order to quantify intervertebral flexion and axial rotation measures. Following ultrasound imaging, an additional rigid body was affixed at the level of L1 in order to quantify the motion occurring exclusively between L1 and S1. The additional trials with the L1 rigid body enabled direct comparison between ultrasound and optoelectronic kinematic measures.

4.2 Participants

Eleven university-aged males and 10 university aged females (n=21) participated in this study. Participants were excluded if they had sought medical treatment or taken two consecutive days off school or work due to neck, trunk, or pelvis pain during the 12 months prior to collection.

Anthropometrics including body weight, height, and bodyfat via hand-held bioelectric impedance analysis (Omron® HBF-306C Fat Loss Monitor, Omron Healthcare, Inc., Bannockburn, IL, USA) were collected. This protocol was approved by the Office of Research Human Participant Review Sub-Committee at York University (Certificate #2018-250). Each participant was provided written informed consent prior to beginning the study. To provide context about the participants, the International Physical Activity Questionnaire (IPAQ) and a custom health questionnaire (including questions about movement habits and exposures) were administered, along with an exit survey that related to participant experience in the study.

4.3   Equipment / Instrumentation

Five NDI 3D Investigator position sensors (3D Investigator™, Northern Digital Inc., Ontario, Canada) and NDI First Principles software (v1.2.4, Northern Digital Inc., Ontario, Canada) were used to detect a total of 24 NDI Smart Markers (battery powered infra-red emitting diodes or IREDs, Northern Digital Inc., Ontario, Canada) placed on the participant and ultrasound transducer. Custom rigid bodies with six Smart Markers each were placed on the spine at the superior dorsal surface of the sacrum (S1 Rigid Body), the SP of the tenth thoracic vertebrae (T10 Rigid Body) to characterize regional spine motion. An additional rigid body was placed over the SP of the first lumbar vertebrae (L1 Rigid Body) following ultrasound imaging. All motion capture data were collected at 90Hz in order to synchronize with 30Hz digital video recordings (after down sampling) for backup purposes. Additional points were digitized on the participants at the right and left anterior superior iliac spines (RASIS, LASIS), posterior superior iliac spines (RPSIS, LPSIS), and C7 SP, as well as four points on the face of the transducer (TRANSD), as shown in Figure 4.1. An example of the rigid body that was used on the spine is shown in Figure 4.2A, and the rigid body configuration for the ultrasound transducer is shown in Figure 4.2B.

An ultrasound unit with a linear transducer was used to capture spine kinematics (Vivid-i™, 9L 2.5-8.0MHz Linear Transducer, 44mm width, GE Healthcare, Illinois, USA; Figure 4.3). Ultrasound operating

frequency was set between 4MHz and 6MHz. The baseline focal point depth for sagittal imaging was set

at the perceived depth of the SP, and for transverse imaging one focal point was set at the perceived

depth of the SP and another focal point was set to the depth of the laminae (settings were optimized for

each participant).
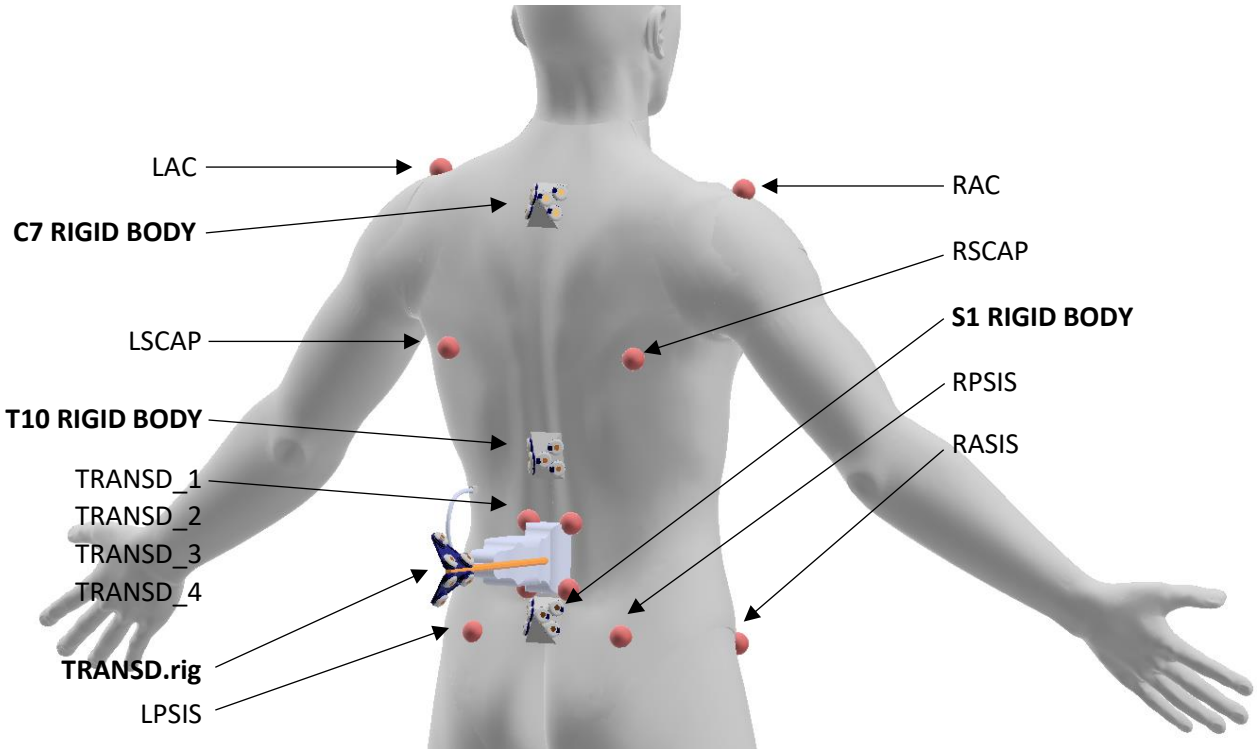
Figure 4.1 – Optical motion capture marker configuration. Labels in bold represent Smart Markers arranged in rigid bodies, whereas red spheres represent digitized points. LAC: left acromion, RAC: right acromion, LSCAP: left scapula, RSCAP: right scapula, LPSIS: left posterior superior iliac spine, RPSIS: right posterior superior iliac spine. (Note: Image of person sourced from GrabCAD online repository (Model: 'Adam_Group_Closed.3dm'). Model of transducer, rigid bodies, and Smart Markers were custom made.)
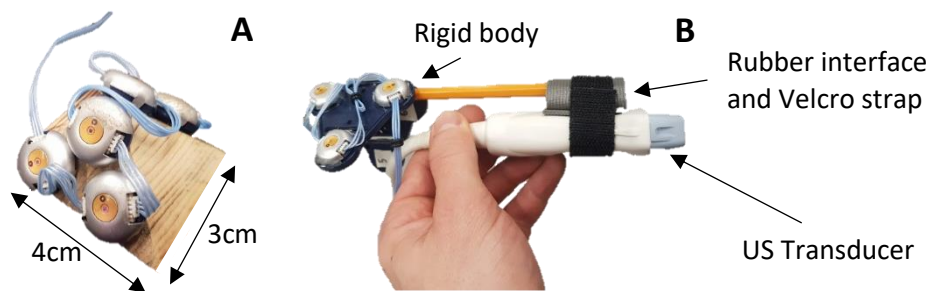
Figure 4.2 – Optical motion capture rigid bodies. A: 6-Smart Marker rigid bodies to be used at S1, T10 & C7. B: 6-Smart Marker rigid body mounted to ultrasound transducer.
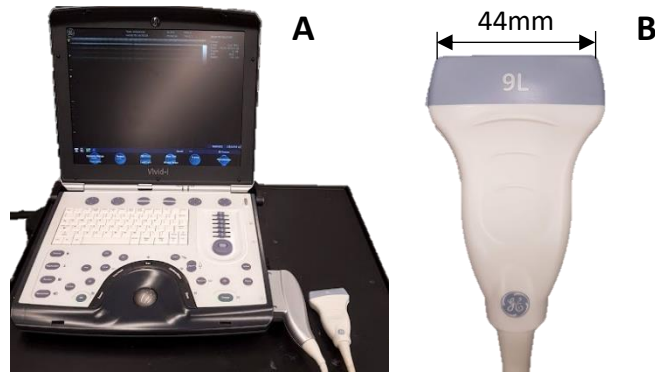
Figure 4.3 – A: GE Vivid i ultrasound unit. B: GE 9L 2.5-8MHz linear transducer.

Other equipment that was used in this research included a padded table, Bosu® ball, Swiss ball, and custom table-top peg board. The padded table and the 60cm Bosu® ball (Bosu® NexGen™ Pro Balance Trainer, Bosu, Ohio, USA) were used to support the participant in their supine flexion position during the error testing protocol as shown in Figure 4.4A. The 30cm Swiss ball was used to support the participant during flexion reference range testing (Figure 4.4B). Following the error testing protocol, the participant completed a series of MMH tasks (Figure 4.5) using the custom table-top peg board (150cm by 76cm) affixed to the table-top by two 13kg clamps. Table height was adjusted for each participant in order to secure them to the table at the height of their ASISs using a ratchet strap and a foam pad for comfort, thereby encouraging motion at the spine. The participant was instructed to place a 2cm-diameter dowel into the various holes to help them hold the required target spine postures.
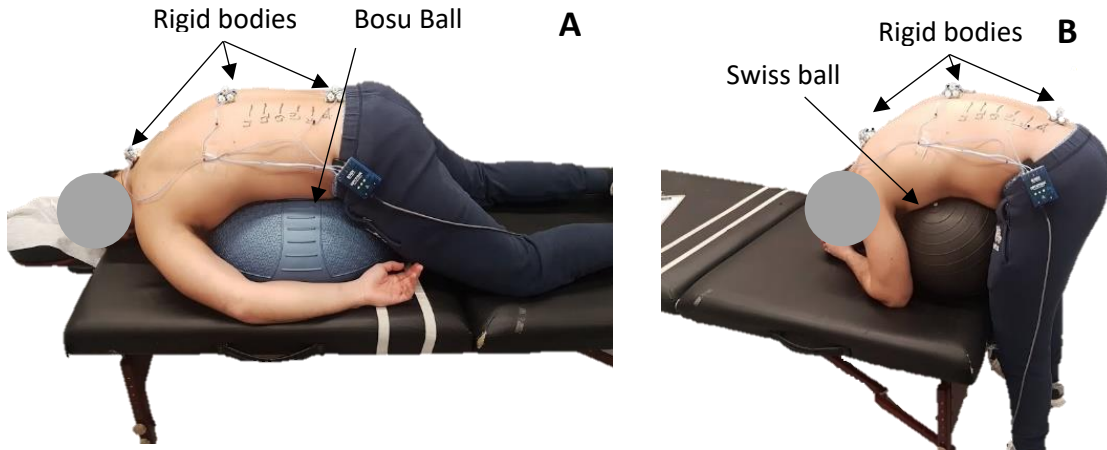
Figure 4.4 – A: Participant laying in a supported flexion posture on a 60cm Bosu® ball for error testing. B: Participant completing flexion reference task by curling spine around a 30cm Swiss ball. Analyzed in addition to MMH tasks. The lines drawn on the spine of the participant indicate the lumbar vertebral levels located with ultrasound with the participant in a neutral standing position (not shown).
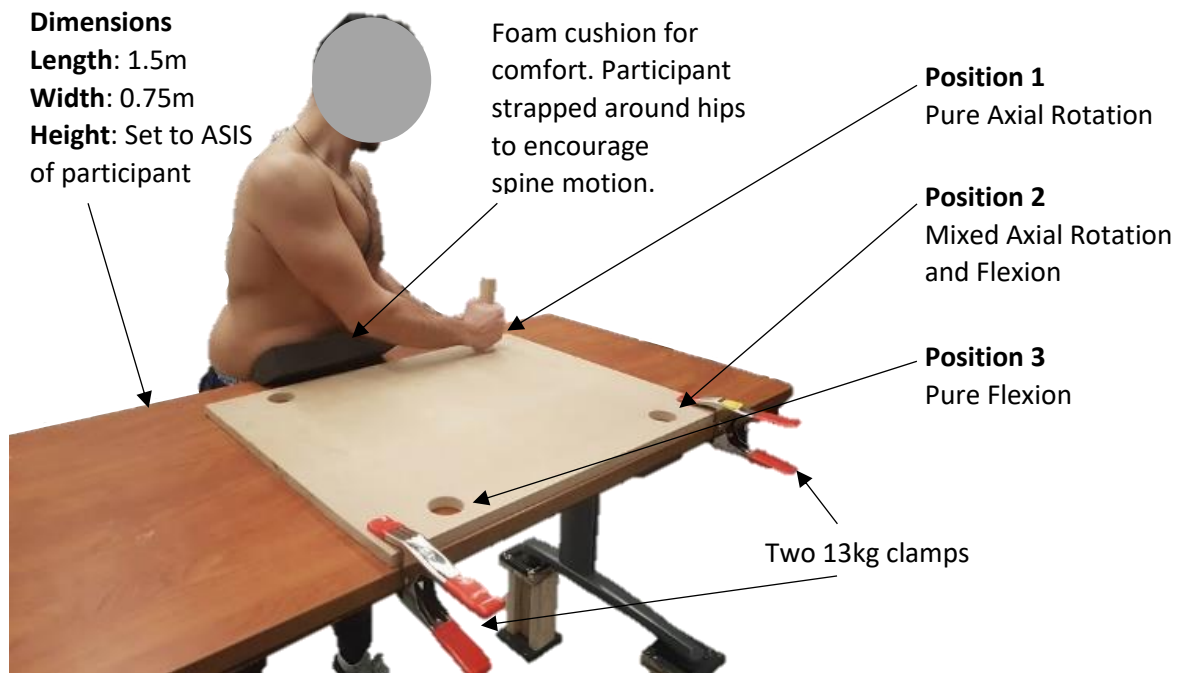
Figure 4.5 – Custom peg board used for MMH task. Two 13kg clamps shown holding board to table. This task is designed to assist the participant in holding various postures.

4.4 Protocol

4.4.1 Overview

The participant was verbally briefed on the experimental protocol and given a consent form, completed the questionnaires, and anthropometrics were collected. The SPs of the participant were identified via ultrasound while in a neutral standing posture and were marked from T10 to S1. Sagittal ultrasound reference images were taken at L1-L2, L2-L3, L3-L4, L4-L5 and L5-S1 in both a standing neutral and a supported flexion posture (trunk supported by a 30cm Swiss ball). Transverse reference ultrasound images were taken at L1, L2, L3, L4, and L5. The participant was then positioned prone on the padded table for error testing. Participants then performed the simulated MMH tasks, which involved surface-based optoelectronic motion capture of the spine in addition to sagittal and transverse ultrasound imaging at all lumbar vertebral levels. Once ultrasound imaging within the MMH tasks was complete, an additional rigid body was affixed at the level of L1 to enable direct comparison to ultrasound (US) measures within this same region. With the additional rigid body in place, MMH and error testing positions were repeated, followed by full flexion, rotation, and lateral bend ROM testing where participants moved to self-identified maximal positions. The affixed rigid bodies were then removed, and participants completed the exit survey.

For discussion purposes, it is helpful to describe the nomenclature of the positions and the various images within these positions. For example, in the simulated pure rotation MMH task (11 series images), a total of 10 ultrasound images were captured. The first five images (11.01-11.05) describe the SP spacing in the test position, which can be compared to SP spacing reference sagittal images taken at the beginning of the experiment. The last five images (11.06-11.10) describe the axial rotation of each vertebrae relative to the S1 rigid body. To obtain relative motion at the L1-L2 joint for example, the rotation at L1 relative to the S1 rigid body was subtracted from the rotation at L2 relative to the S1 rigid body.

11.01 – Sagittal image over L1 and L2 which yielded the spacing between L1 and L2 SPs.
11.02 – Sagittal image over L2 and L3 which yielded the spacing between L2 and L3 SPs.
11.03 – Sagittal image over L3 and L4 which yielded the spacing between L3 and L4 SPs.
11.04 – Sagittal image over L4 and L5 which yielded the spacing between L4 and L5 SPs.
11.05 – Sagittal image over L5 and S1 which yielded the spacing between L5 and S1 tubercle.

11.06 – Transverse image at L1 which yielded L1 axial rotation relative to the S1 rigid body via mocap.
11.07 – Transverse image at L2 which yielded L2 axial rotation relative to the S1 rigid body via mocap.
11.08 – Transverse image at L3 which yielded L3 axial rotation relative to the S1 rigid body via mocap.
11.09 – Transverse image at L4 which yielded L4 axial rotation relative to the S1 rigid body via mocap.
11.10 – Transverse image at L5 which yielded L5 axial rotation relative to the S1 rigid body via mocap.

4.4.2   Error Testing

For the error testing, the participant lay prone on the padded table in three supported positions: neutral, flexion and axial rotation. The goal was not to have each participant in precisely the same posture, but rather to elicit a stable position where repeated measures could be compared. Sagittal error testing was conducted in the neutral and supported flexion positions at the level of L1-L2, while transverse error testing was conducted in the neutral and supported axial rotation positions at the level of L1 to assess the robustness and repeatability of these measurement methods. An ultrasound M-mode collection (ultrasound video loop) was synchronized to begin with motion capture when the ideal image was found. From this ideal image, the transducer was systematically tilted or translated to induce error into the image. An image acquisition window was later obtained from this tilting and translating range. An illustration of the error testing protocol is shown in Figure 4.6, and a three-dimensional model of this same process is provided in Figure 4.7 to help clarify the protocol. The resulting M-mode loop contained the ideal, last-measurable, and lost images which were retrieved after the collection for analyses. Criteria for these image classifications was provided in Table 4.1 and sample images associated with these classifcations was provided in Figure 4.8. Lost images generally contained identifiable skin and adipose but otherwise contained no intelligible anatomical landmarks for measurement.
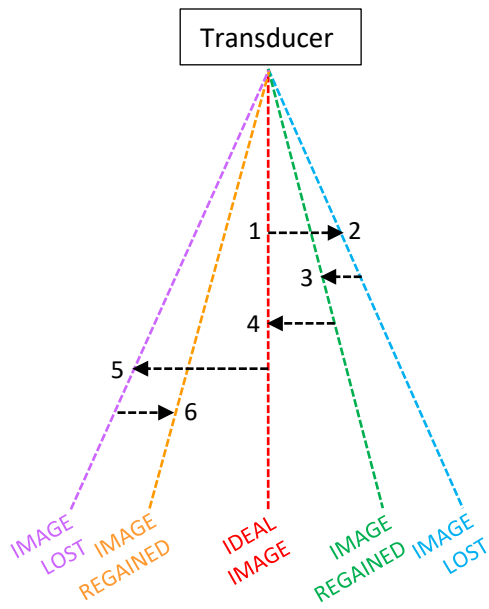
#	Description of Error Testing Protocol
1	Capture an ideal M-mode US loop (red)
2	Tilt towards investigator until image is lost (blue).
3	Last measurable image pulled from US loop after collection (green).
4	Capture an ideal M-mode US loop (red)
5	Tilt away from investigator until image is lost (purple).
6	Last measurable image captured from US loop after collection (yellow).

Figure 4.6 – Illustration of error testing protocol used to investigate the possibility of acquiring an image which appears readable but yields inaccurate results in terms of vertebral orientation (robustness). As well, measurements from ideal image repeats are compared to one another to assess repeatability.
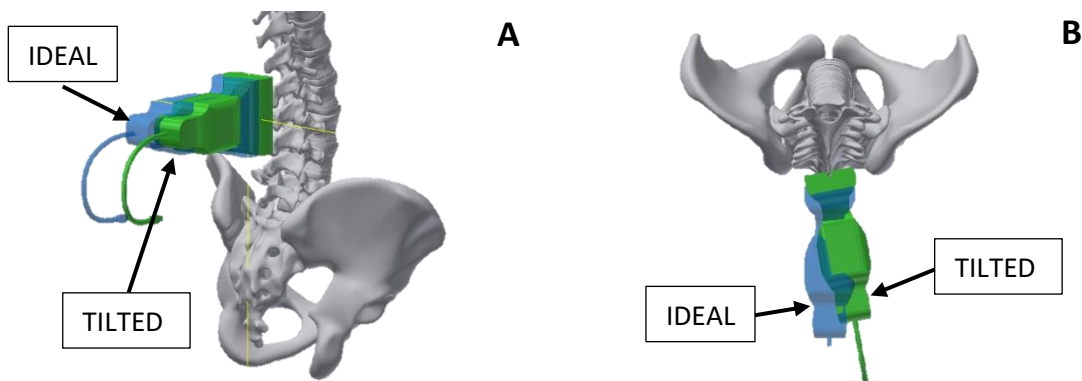
Figure 4.7 – A: Posterolateral view of error testing for sagittal plane ultrasound imaging. Flexion images were acquired with this sagittal transducer orientation. B: Transverse plane view looking inferiorly. The green transducer shows the tilted position of the transducer.

Table 4.1 – Classification and associated criteria for sagittal and transverse ultrasound images.

Image Classification	Sagittal Image	Transverse Image
Ideal	• Contains clear echoes from two SPs *AND* • Distinct apices	• Contains clear approximately 9-10mm echo from SP *AND* • Contains clear echoes from laminae *AND* • Laminae are perpendicular to image
Lost	• Contains less than two echoes of SPs *OR* • No distinct apices	• Contains no echo from SP *OR* • Contains no echo from laminae
Last Measurable	• Contains echoes from two SPs *AND* • Less distinct apices	• Contains echo from SP *AND* • Contain echoes from laminae
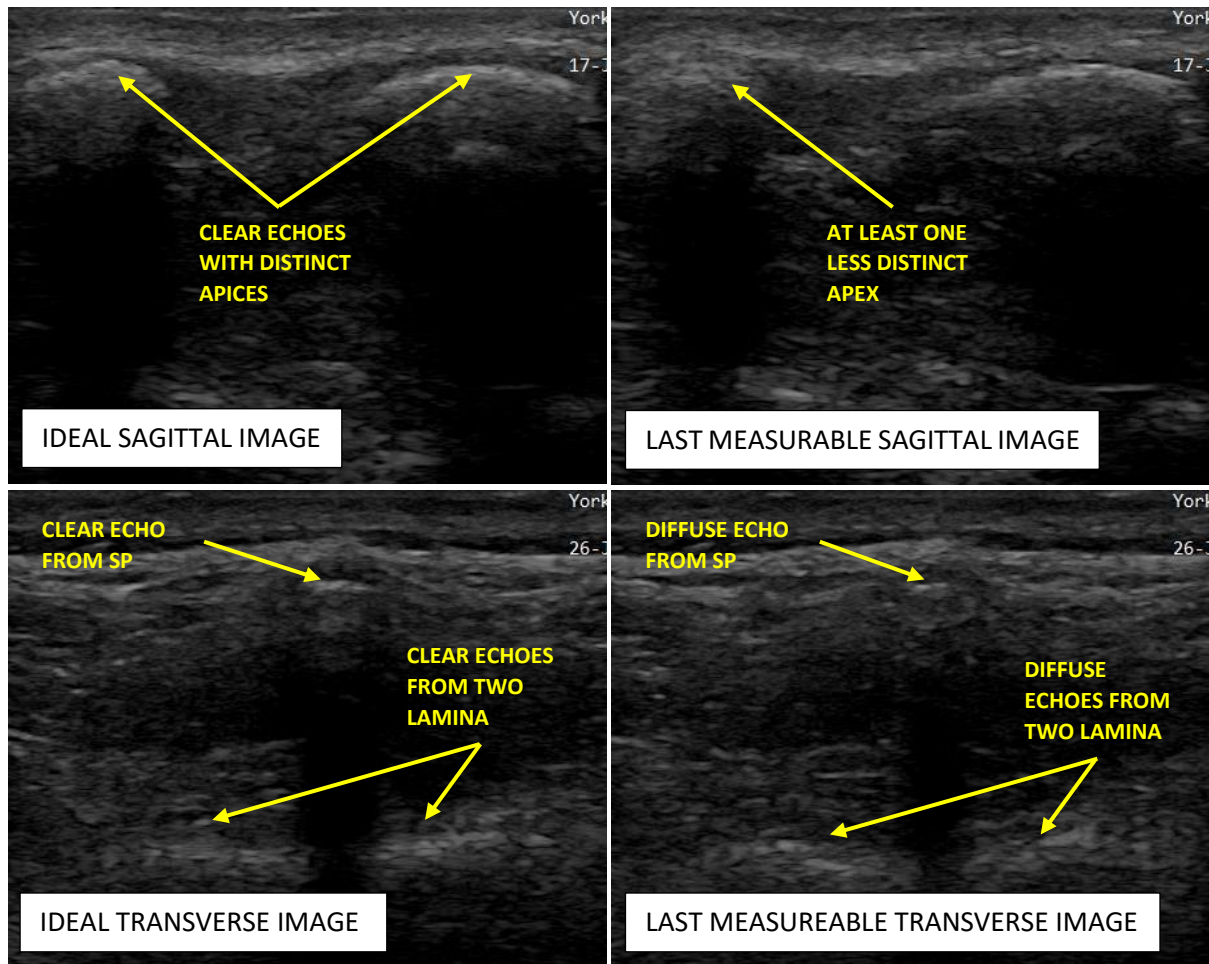
Figure 4.8 – Examples of images fitting ideal and last measurable classification from Table 4.1 above. Top of each image was the skin surface.

4.4.3 Simulated MMH Task

Following error testing, the participant completed the simulated MMH task involving the custom pegboard and reaching tasks which elicited three static spine positions: predominant axial rotation, combined axial rotation and flexion, and predominant flexion. From pilot work, the predominant axial rotation position was developed to elicit axial rotation without (or with very little) confounding flexion motion from participants. Likewise, the isolated flexion position permitted the measurement of lumbar flexion without axial rotation confounding the images. The combined axial rotation and flexion position induced combined flexion and axial rotation while sagittal and transverse ultrasound images of the lumbar vertebrae were obtained. The participant's pelvis was restrained and supported with a strap during these tasks to encourage movement from the spine, as was done by Drake and Callaghan (2008). Surface-based motion capture and ultrasound images (sagittal and transverse) were captured at all lumbar levels (L1-L5) as the participant held each position for approximately five minutes (facilitated by the pegboard). The ultrasound image acquisition proceeded like the ideal imaging methods described above for error testing (see section 4.4.2). The ultrasound method was found to be repeatable during pilot work, and so repeat images in the MMH task were not obtained to reduce the total duration participants maintained the required postures and overall total collection duration. Further, repeatability of the experimental data were assessed prior to the analysis of the MMH task, and these experimental data supported that repeat images were not required if the duration of image acquisition was controlled (which it was in the MMH procedure). Single ideal images (identified by clear and highly echoic anatomical features) were acquired at L1 through S1 in sagittal (to quantify flexion) and L1 though L5 in transverse orientations (to quantify axial rotation) in each position. Regional motion capture was collected throughout ultrasound imaging and was compared to ultrasound imaging results. See *Appendix A – Error and Repeatability Protocols* for step-by-step diagrams illustrating transducer placement during ultrasound error and repeatability protocols and *Appendix B – Detailed* for stepwise detail regarding data collection.

4.5 Data Processing

4.5.1 Motion Capture

Surface-based (optoelectronic) motion capture data from sacrum (S1 Rigid Body) and tenth thoracic (T10 Rigid Body) rigid bodies were used during error testing and the simulated MMH task. During error testing, motion capture was collected to ensure the participant remained static during US M-mode collection and to provide orientation data of the transducer during the acquisition of ideal and lost images. The sagittal plane tilting acquisition window was calculated by taking the difference between the longitudinal axis orientations for ideal and lost images. A similar process was followed to solve for the sagittal plane translation acquisition window, in addition to the tilting and translating windows for the transverse orientation (Figure 4.9). In the MMH trials, surface-based motion capture was used to compare the sum-total of ultrasound measurements (discussed in section 4.5.3) across this same region (L1 to S1 - a total of 5 joints). All surface-based motion capture data were analyzed using Visual3D (v6.01.34, C-Motion Inc., Germantown, MD).
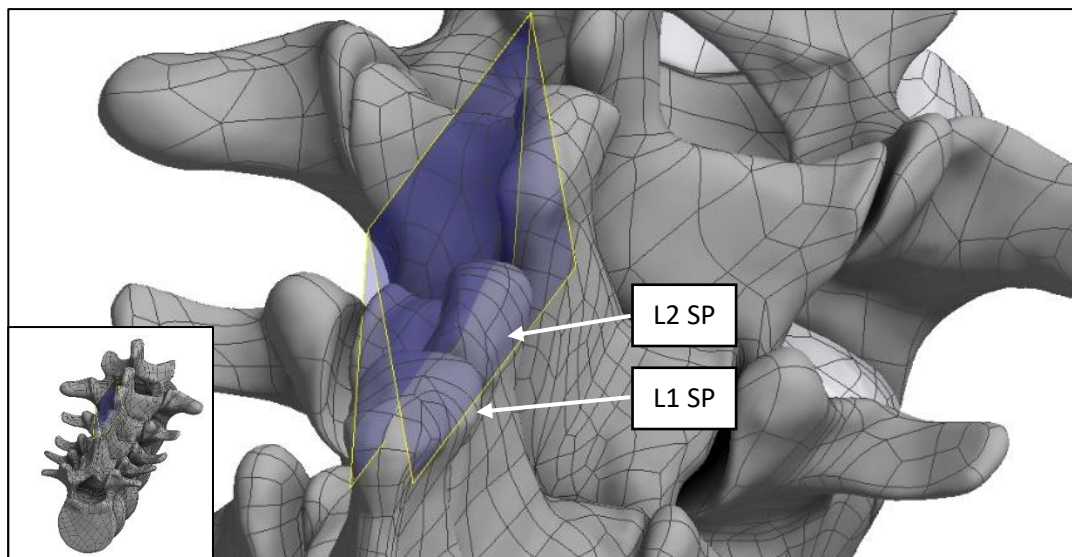
Figure 4.9 – A 3D spine model used to visualize the tilting acquisition window (represented by blue planes). Outside of this window, the ultrasound slice will not intersect the SP and the returning echo will be weak or non-existent. This theoretical acquisition window was investigated experimentally.

4.5.2 Sagittal Ultrasound Images

The method of processing the sagittal ultrasound images was adapted from van den Hoorn et al. (2016) and involved the US images being analyzed using MicroDicom software (MicroDicom ©, version 2.7.9, build 101). Images were presented in the order collected, with image numbers superimposed to provide context to the rater (i.e. neutral sagittal plane image). First, linear measurements were made between the perceived peaks of the SPs. These peaks generally appeared as two highly echoic semi-ellipses, 15-25mm in length and 5-15mm beneath the skin surface. An illustration of this measurement process is shown in Figure 4.10 and Figure 4.11. This linear spacing measurement was compared within participants across different tasks.
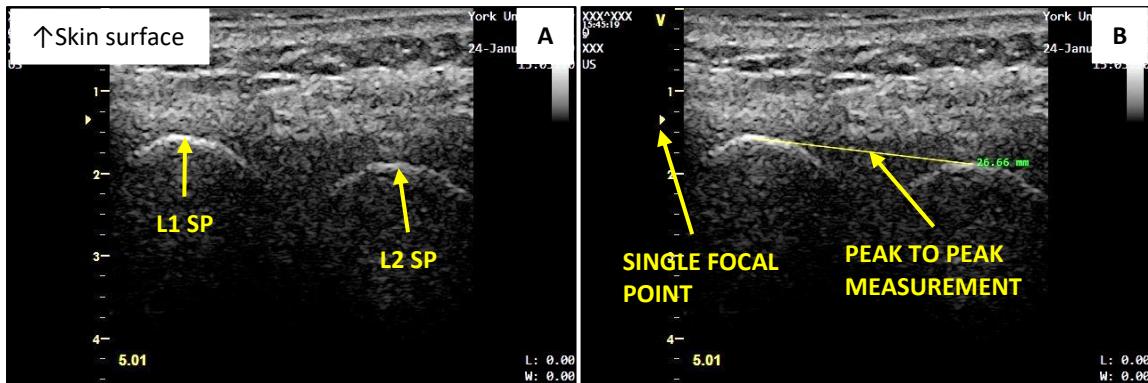
Figure 4.10 – A: Original, unprocessed image. B: SP spacing measured between the perceived peaks of the SPs. This measure was used to determine the extent of flexion at each vertebral joint.
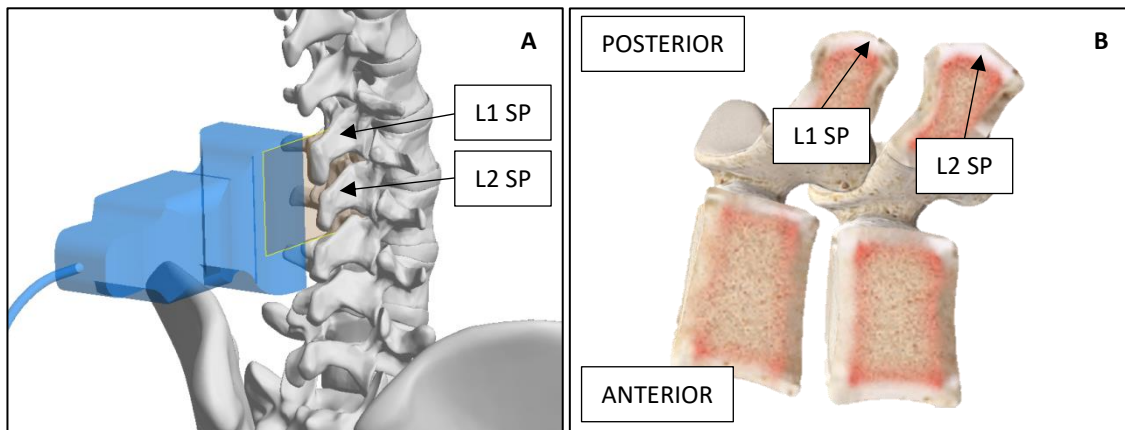
Figure 4.11 – A: Anatomical posterolateral view of L1-L2 during sagittal imaging process. B: Anatomical image showing sagittal section view of L1-L2 SPs.

For example, in the standing neutral position, spacing between the L1 and L2 SPs is 25mm and 34mm in the full flexion trial. This provides a flexion range of 9mm. With this information, the MMH task can be evaluated against this full flexion range as shown in Ex. 1 where assuming the MMH task displayed 31mm SP spacing:

Ex. 1
$$\% flexion = 1 - \frac{full\ flexion - MMH\ flexion}{full\ flexion - neutral} \ x\ 100\%$$

$$= 1 - \frac{(34mm - 31mm)}{(34mm - 25mm)} \ x\ 100\%$$
$$= 66.6\% \ full\ flexion\ at\ L1 - L2$$

4.5.3 Transverse Ultrasound Images

The method for processing transverse ultrasound images was adapted from Mayberry et al. (2018) and Suzuki et al. (1989), and involved analyzing the ultrasound images using MicroDicom software (MicroDicom©, version 2.7.9, build 101). Images were presented in the order collected, with image numbers superimposed and therefore imaging context was known to the rater. First, the SP was identified in the ultrasound image. It generally appeared as a narrow (approx. 9-10mm wide) and highly echoic surface approximately 5-15mm beneath the skin surface. While imaging, the intention was to have the shadow from this process be as thin and dark as possible (strong echo). Secondly, the laminae were also identified in the image as a strong, horizontal, and bilateral echo, as shown in Figure 4.10. This indicated that the transducer was roughly perpendicular to the vertebra. An example of how intervertebral rotation was calculated is shown in Ex. 2 below.

Ex. 2   Use Visual3D to establish local coordinate system between T10 and S1 rigid bodies in order to establish a local longitudinal axis about which axial rotations may be calculated. Use Visual3D to calculate ultrasound orientation about this axis.
$$Transducer\ orientation\ about\ local\ logitudinal\ axis, R_{Z_{MOCAP}}$$
$$For\ this\ example, assume\ R_{Z_{MOCAP}} = 99°$$

Ultrasound image analysis yielded the degree to which the vertebra was rotated within the image. In an ideal case, this value is zero (and therefore the orientation of the transducer is a

mirror image of the vertebral orientation) but in some cases, an image with zero perceived vertebral rotation is not achievable. Using data from Figure 4.12,

$$Vertebral\ body\ orientation\ in\ imaging\ plane, R_{Z_{US}}$$
$$= 90° - 88.70°$$
$$= 1.13°\ (clockwise)$$

The cumulative orientation of the transducer can be calculated as follows:
$$R_{Z_{TOTAL}} = 99°\ CCW\ (mocap) + 1.13°\ CW\ (US)$$
$$= 97.87°\ CCW$$

Therefore, the L1 vertebral body is oriented at 97.87° relative to the local coordinate system. This process was repeated for L2, L3, L4 and L5 vertebral bodies (S1 orientation is established via a rigid body) in order to establish axial rotation at each joint, i.e. L1-L2 etc.

If we assume that $R_{Z_{TOTAL}}$ for $L2 = 94°\ CCW$, then the total axial rotation at L1-L2 is:
$$= 97.87° - 94°$$
$$\cong 4°$$
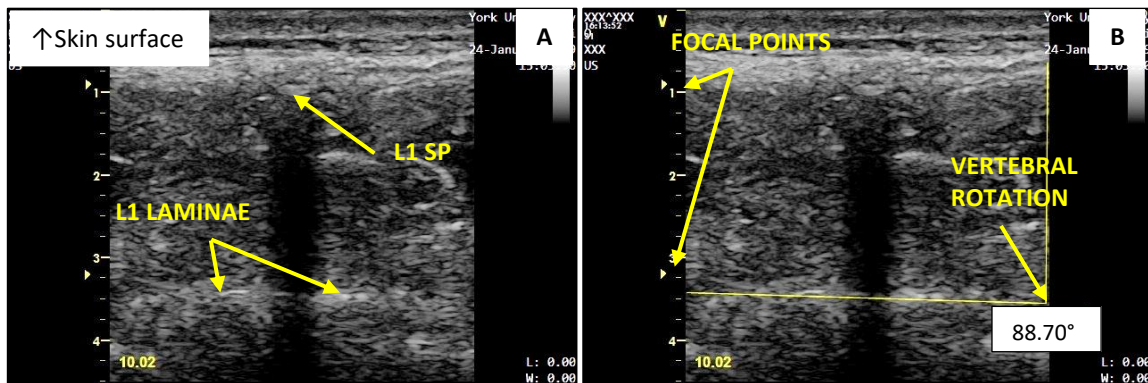
Figure 4.12 – A: Ultrasound image showing transverse view of SP and corresponding shadow projection. B: Analyzed image showing orientation of the vertebrae relative to the imaging frame (88.70°) in addition to the two focal point depth settings used when acquiring transverse plane images.
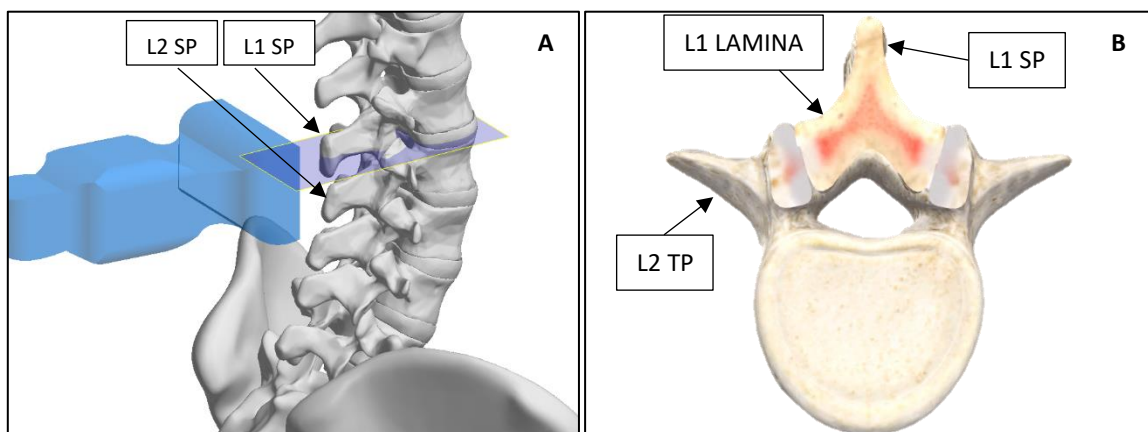
Figure 4.13 – A: Anatomical posterolateral image demonstrating the transverse imaging process. B: Anatomical image showing a transverse (sectioned) view of L1-L2 at the level of the L1 SP and L1 laminae. The transverse processes of the inferior vertebrae are also visible in this section view, but they are not targeted due to depth and imaging difficulty.

4.6 Data Analysis

4.6.1 Repeatability

Repeatability was defined as the "closeness of the agreement between the results of successive measurements of the same measurand carried out under the same conditions of measurement" (BIPM, 2008). For the sagittal imaging method, a three-way mixed ANOVA ($\alpha = 0.05$) was applied to the images collected from 20 participants to examine the effect of sex (two levels – male = 10, female = 10), position (two levels – neutral = 10, flexion = 10), and image repeat (4 levels – ideal1 n = 20, ideal2 n = 20, ideal3 n = 20, ideal4 n = 20) on SP spacing measurements at the L1-L2 joint. Homogeneity of variance was tested via Levene's Test of Equal Variance, and sphericity was tested via Mauchly's Test of Sphericity and a correction factor was applied if significant. Significant interactions were reported when found and main effects were reported only in the absence of significant interactions. One participant was removed from this portion of the analysis due to a missing US image. For the transverse imaging method, a three-way mixed ANOVA ($\alpha = 0.05$) was run on a sample of 16 participants to examine the effect of sex (two levels – male = 8, female = 8), position (two levels – neutral = 8, flexion = 8), and image repeat (4 levels – ideal1 n = 16, ideal2 n = 16, ideal3 n = 16, ideal4 n = 16) on axial rotation repeated measurements. Homogeneity of variance was tested, and a correction factor was applied to degrees of freedom if violated. Significant interactions were reported if found and main effects were reported only in the absence of significant interactions. Five participants were removed from this portion of the analysis due to incomplete motion capture data.

The repeatability coefficient as outlined by Bartlett & Frost (1.96 × √2 × within-participant SD) (2008) was also used to assess both imaging methods and provides an idea of the within-participant repeatability. The repeatability coefficient is a number which describes the maximum difference between two successive measurements for 95 measurements out of 100. A two-way mixed-effects model was also used to evaluate the intraclass correlation coefficients (ICC) of repeated image analyses for both imaging

methods to assess the reliability of the rater. The ICC is presented in the repeatability section since intrarater reliability was considered a contributor to repeatability error.

4.6.2   Robustness

For the sagittal imaging method, a three-way mixed ANOVA (α = 0.05) was run on a sample of 20 participants to examine the effect of sex (two levels – male = 10, female = 10), position (two levels – neutral = 10, flexion = 10), and image repeat number (4 levels – diff1, n = 20, diff2 n = 20, diff3 n = 20, diff4 n = 20) on measurement differences between ideal and non-ideal images at the L1-L2 joint. Homogeneity of variance was tested via Levene's Test of Equal Variance, and sphericity was tested via Mauchly's Test of Sphericity and a correction factor applied if significant. To assist with visualizing the data, the differences in ideal vs non-ideal images were illustrated via a Bland-Altman plot.

4.6.3   Image Acquisition Window

The image acquisition windows were tested via four separate three-way ANOVAs ($\alpha = 0.05$) on a sample of n=21 for 7- and 9-series tilting, n=19 for 7- and 9-series translation, n=19 for 8- and 10-series tilt, and n=17 for 8- and 10-series translation. The ANOVAs investigated the effect of sex (two levels), position (two levels), and direction of 1) tilt (two levels) or 2) translation (two levels) on the size of the acquisition window for the sagittal method at the L1-L2 joint and the transverse imaging method at L1. Homogeneity of variance was tested via Levene's Test of Equal Variance, although group sizes were equal and their departures from this assumption were not problematic.

4.6.4   MMH Task Sagittal Imaging

Sagittal plane ultrasound images for the MMH tasks were analyzed in terms of both relative and absolute ROMs on each n=20 participants individually. One participant was removed from the analysis due to poor quality US images at L4-L5. Relative ROM was calculated by expressing each joint-level ROM (in mm) to the participant's total ROM across all levels (total ROM in mm). For example, if a participant demonstrated 5mm change in SP spacing at L1-L2, 5mm at L2-L3, 5mm at L3-L4 and 10mm at L4-L5, then

the relative change at L1-L2 would have been 5mm / (5mm + 5mm + 5mm + 10mm) = 20% ROM at L1-L2 for this participant in this task. Similar calculations would be conducted for the remaining lumbar joints. Absolute ROM was simply measured as millimeters of change in spacing between all SPs within each participant (as in the above example, L1-L2 = 5mm, L2-L3 = 5mm etc). Both absolute and relative measures were investigated for the presence of outliers and were considered outliers if the ROM lay beyond 1.5x the interquartile range (IQR). Box and whisker plots were also generated for surface-based optoelectronic motion capture measurements of the MMH tasks to enable comparison of outlier detection between ultrasound and surface-based optoelectronic motion capture.

4.6.5 MMH Task Transverse Imaging

A two-way ANOVA (α=0.05) was run on a sample of n=10 participants with additional motion capture data to investigate the effects of participant sex (two levels), task (three levels) on the difference between ultrasound and surface-based optoelectronic motion capture measures of axial rotation directly within the L1-S1 region. A confidence interval was established to describe the difference between measures. Lastly, a frequency plot was generated to describe the measurement differences between ultrasound and optoelectronic motion capture.

5   RESULTS

This section will first present the results of the ultrasound error testing protocols for repeatability and robustness followed by the results from the MMH tasks which involved axial rotation, lumbar flexion, or a combination of both flexion and axial rotation. Based on previous research, theoretical analyses, and current research findings, repeatability (which is a function of imaging repeatability and intrarater reliability) and robustness were suspected to be the main sources of error within the system. Repeatability was assessed by comparing sequentially captured ideal images, while robustness was assessed by comparing sequentially captured ideal images to images which contain systematically induced error. An imaging acquisition window was presented, which described the tolerable amount of transducer movement which preserved repeatability. All participant data were sorted by largest SP ROM at L1-L2 during the flexion reference task.

5.1   Repeatability

Ideal images taken during the error testing protocol (see section 3.4.2 – Error Testing) provided a unique opportunity to assess repeatability for both the sagittal and transverse images. Recall that each position (neutral, flexion and axial rotation) yielded four image repeats of the same anatomical information while the participant remained in the prescribed static posture (held to within an average SD of 0.73° in flexion and 0.38° in axial rotation, observed motion was likely due to breathing). Ideal image measurements, taken in short succession, should not be statistically different. A repeatability coefficient was also established to describe the repeatability within each participant.

5.1.1   Sagittal Imaging

A three-way mixed ANOVA was conducted to investigate the relationship between participant position (two levels), sex (two levels), and image repeat number (four levels) on SP spacing measurements. Mauchly's test indicated that the assumption of sphericity had been violated $\chi^2(5) = 31.48, p < 0.001$ therefore degrees of freedom were corrected using Greenhouse-Geisser estimates of

sphericity. The results failed to show any significant within participant interaction effects $F_{(1.9,108)} < 1.970$, p>0.148 or within participant main effects $F_{(1.9,108)} = 0.960$, p = 0.386. These results suggest that successive image measurements were repeatable on average. The mean (SD) for repeats 1 through 4 across 20 participants were 29.8mm (3.88), 29.6mm (4.03), 29.6mm (4.17), 29.7mm (4.26).

There was a significant between participant main effect for position $F_{(1,36)} = 4.804$, p=0.035, which suggests that in the flexion position, the average SP spacing was larger, as expected. The mean (SD) for each position across 20 participants were 28.3mm (4.07) for neutral and 31.0mm (3.50) for flexion.

A repeatability coefficient was also computed ($SD\ of\ differences \cdot \sqrt{2} \cdot 1.96$) for the neutral and flexion trials to describe the variability within each participant (Figure 5.1). In the neutral position, the highest (worst-case) repeatability coefficient was 6.16mm, the lowest (best-case) was 0.69mm, the average was 1.90mm and 80% of repeatability coefficients were less than 3mm. A repeatability coefficient of 6.16mm (for example) indicates that the difference in SP spacing from one trial to the next would be at most 6.16mm for 95% of the trials. For the flexion position, the highest repeatability coefficient was 3.66mm, the lowest was 0.54mm, the average was 1.72mm and 80% of the repeatability coefficients were less than 3mm.

Figure 5.1 – Left: Histogram of laying neutral spine (7-Series) repeatability coefficients for all participants. The average repeatability coefficient in the neutral position was 1.90mm and over 80% of participants had a repeatability coefficient of 3mm or less (80% indicated by grey dashed line). Right: Histogram of prone laying spine flexion (9-Series) repeatability coefficients for all participants. The average repeatability coefficient in the flexion position was 1.72mm and over 80% of participants had a repeatability coefficient of 3mm or less (80% indicated by grey dashed line).

In addition to statistical measures, it can be helpful to consider each participant's measurement error in the context of various ROMs. To briefly summarize this concept, the participant had four image repeats taken in neutral, and four in a supported flexion position. If the participant displayed small ROM at the L1-L2 joint, had high variability in the measurements at that joint or some combination thereof, the method would fail to distinguish these between two positions (Figure 5.2).
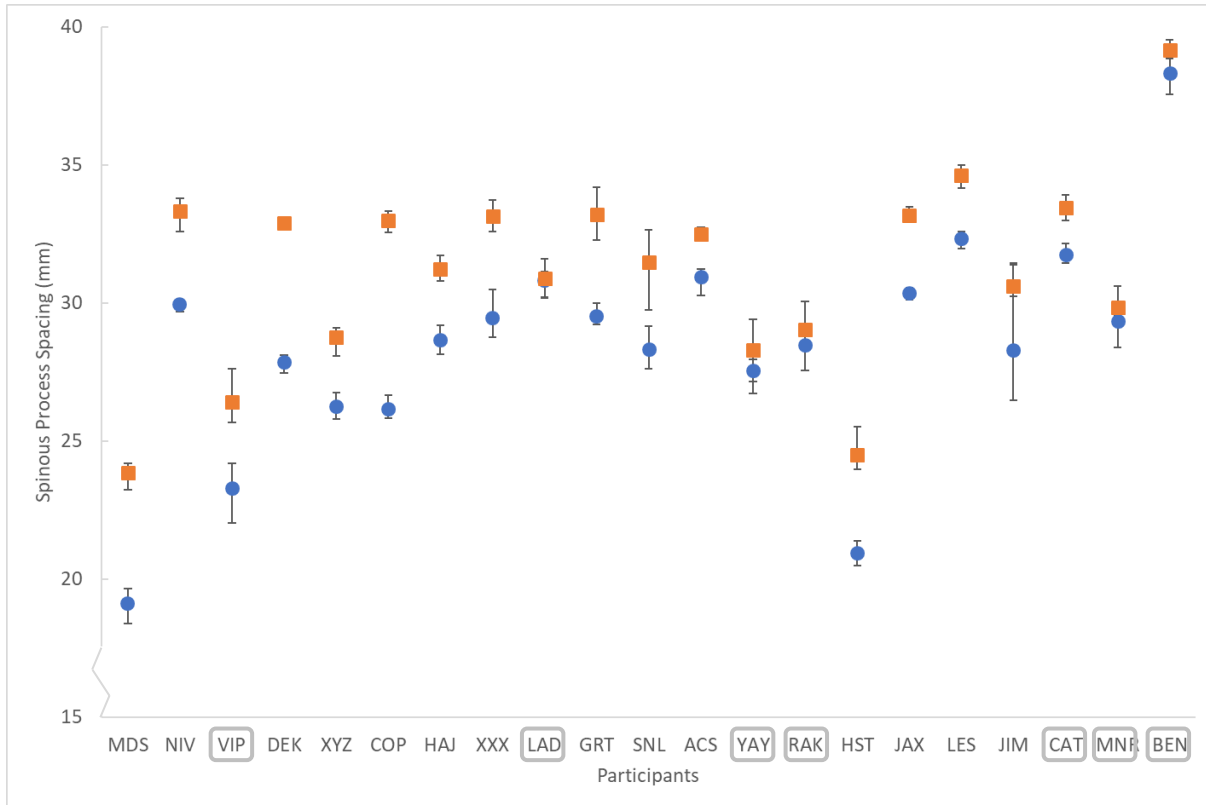
Figure 5.2 – Blue circles represent average SP spacing during neutral laying. Orange squares represent average SP spacing in the laying flexion trial (approximately 40% flexion). Error bars show min and max. Overlap of measurement ranges indicates failure to distinguish one position from the other (participant codes circled in grey). Dependent axis begins at 15mm to improve the visibility of differences in SP spacing between positions.

Measurements were considered repeatable when the range of spacing measurements did not overlap with a range of spacing measurements in the second position (a function of joint ROM and measurement variability). The least repeatable participant was participant LAD whose average SP spacing was 30.8mm (range: 30.5-31.3mm) in a neutral laying position and an average of 30.9mm (range: 30.0-31.9mm) in the flexion laying position. For this participant, a posture of 40% flexion across the L1-S1 region

(measured by surface-based optoelectronic motion capture) elicited a mere 0.09mm change in average SP spacing at L1-L2 as measured by ultrasound (i.e. limited ROM at this joint in this participant for this task). However, the *range* of measurements for the neutral images was 0.75mm which represents over 8 times the amount of actual motion measured at the joint between positions. Therefore, for participant LAD, the amount of error was unacceptable as the US measurement system could not distinguish between neutral laying and 40% flexion. On the other hand, for participant HST, the neutral laying posture elicited an average SP spacing of 21.0mm (range: 20.7-21.1mm) while the laying flexion position showed an average SP spacing of 24.5mm (range: 24.3-24.8mm). In this case, a posture of 40% flexion across the L1-S1 region elicited a 3.6mm change in average SP spacing and the range of measurements in the neutral position was 0.43mm which represents only 12.5% of the measured ROM at the joint between positions. Therefore, for participant HST, this amount of error is acceptable as the ultrasound measurement system can distinguish between neutral laying and 40% flexion. In fact, by linear interpolation, this amount of error would only fail to distinguish between positions of neutral and less than 5% flexion in participant HST.

Analyzing the joint ROM and measurement variability for all participants, it was possible to distinguish between neutral and a 40% flexion position in 14 of 21 participants (Figure 5.3). By linear interpolation, a change in position of 5% flexion could be distinguished in one participant (HST), 10% flexion could be distinguished in seven (HAJ, XXX, COP, GRT, NIV, JAX and MDS) and 20% flexion could be distinguished in two participants (LES and DEK). Seven of 21 participants had a measurement range which overlapped the movement range between neutral and 40% flexion, and therefore could not be considered repeatable for this task. Of the seven participants who were not considered repeatable in the 40% flexion position, five of them displayed ranges of motion which fell below the average by more than 1SD. This suggests that the poor repeatability in these five participants was mostly due to the small ROM at the L1-L2 joint and was not largely related to imaging ability or analytical ability of the imager/rater. One of seven

displayed a range of measurements which was above the average range by more than 1SD. These results suggest that imaging and/or analysis was the main source of error in this participant. The remaining one participant displayed above average measurement range and below average ROM however these variations were both less than one SD from the mean.
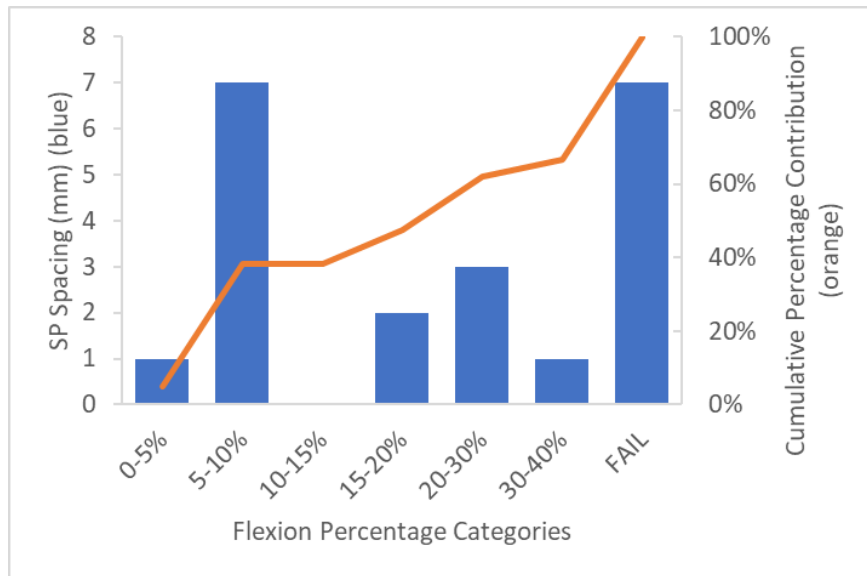
Figure 5.3 – Distribution of the amounts of flexion that could be distinguished within participants based on the range of their measurements and the amount of motion they produced at the L1-L2 joint. 67% of participants could distinguish 40% or less. In nearly 40% of participants, it was possible to distinguish 10% flexion or less. In seven participants (33%), 40% flexion could not be distinguished from neutral due to overlapping measurement ranges.

An ICC was calculated to evaluate the reliability of the rater in analyzing images. The reliability of the rater was distinct from the assessment of overall repeatability (analyzed previously in section 5.1.1 via ideal image repeats) as the analysis of reliability isolates image analysis error from image acquisition error. The 95% CI for the sagittal imaging method was 0.939 to 0.958 which indicates excellent reliability (Koo and Li, 2016).

5.1.2   Transverse Imaging

Repeatability error in the transverse orientation was assessed like the sagittal method in Section 5.1.1. A three-way mixed ANOVA was run to investigate the relationship between participant position (two levels), sex (two levels), and image repeat number (four levels) on vertebral orientation. Mauchly's test indicated that the assumption of sphericity had been violated $\chi^2(5) = 17.58, p = 0.004$ therefore degrees of freedom were corrected using Greenhouse-Geisser estimates of sphericity. The results showed a significant within participant interaction effect for Repeat $\times$ Sex $F_{(2.07,57.9)} = 4.10$, p = 0.020. No significant within participant main effects were found $F_{(2.07,57.9)} < 2.02$, p > 0.14 however a significant between subject main effect was found for sex $F_{(1,28)}$ = 7.08, p = 0.013 which suggests that measurements differed significantly between males and females. A post hoc pairwise comparison with Least Squares Difference correction was run separately for males and females to investigate the Repeat $\times$ Sex interaction and more precisely identify the differences between ideal image repeats. Repeats one through four did not differ in males (p = 0.612) but a significant difference (p < 0.024) was found only in females between ideal image repeats one and two (difference of 0.41°), one and three (difference of 0.81°, and one and four (difference of 1.4°). There appeared to be a consistent increase in measurements across time which may suggest that duration of image acquisition may affect imaging repeatability in females.

A repeatability coefficient was computed for the neutral and axially rotated trials. In the neutral position, the highest repeatability coefficient (worst-case) was 6.53°, the lowest (best-case) was 0.61°, the average was 3.04° and 80% of the participants had repeatability coefficients of 5° or less. A repeatability coefficient of 6.53° (for example) implies that the difference in axial rotation from one trial to the next would be at most 6.53° for 95% of the trials. For the axially rotated position, the highest repeatability coefficient was 6.41°, the lowest was 0.67°, the average was 2.88° and 80% of participants had repeatability coefficients of 4° or less (Figure 5.4).
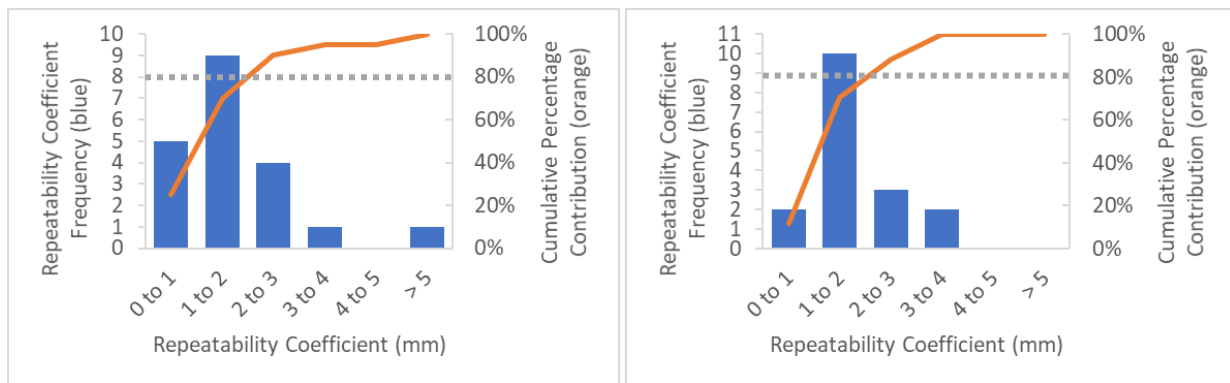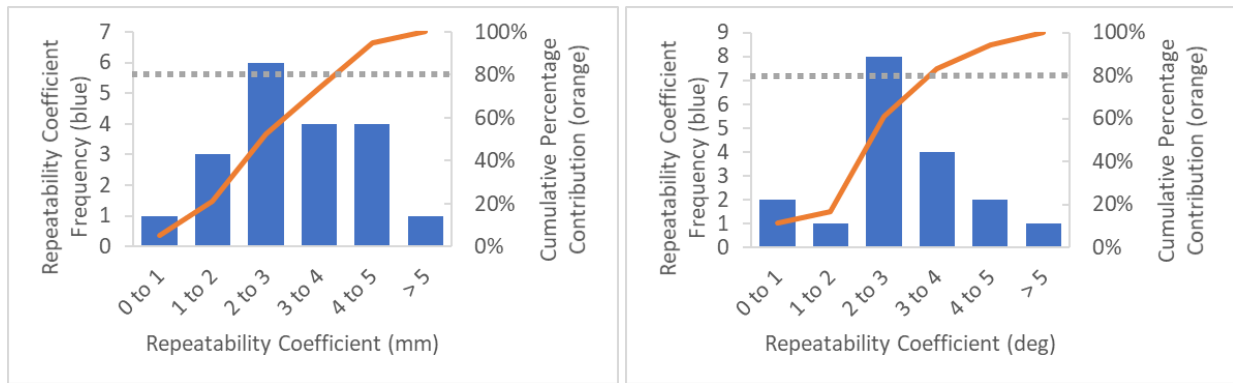
Figure 5.4 – Left: Histogram of laying neutral spine (8-Series) repeatability coefficients for all participants. Participants had an average repeatability coefficient of 3.04°, and over 80% had a repeatability coefficient of 5° or less (80% indicated by grey dashed line). Right: Histogram of laying axial rotation (10-Series) repeatability coefficients for all participants. Participants had an average repeatability coefficient of 2.88° and over 80% had a repeatability coefficient of 4° or less (80% indicated by grey dashed line).

Interpreting these results in the context of physiological ROM helps to determine whether these results would be acceptable in practice. White and Panjabi (1978) measured approximately 2° of axial rotation ROM at each intervertebral joint from L1 down to L5, and 5° at L5-S1. Fujii et al. (2007) reported approximately 1.5° at each lumbar level, including L5-S1. Therefore, with an average repeatability coefficient of 2.88° in the axially rotated positions, 1.5-2° of axial rotation could not be reliably measured in the L1 to S1 intervertebral joints. Only four participants achieved a repeatability which was low enough to reliably measure movement on the order of 2° in the neutral position and only three participants achieved the same in the axially rotated position. These results suggest that it was challenging to acquire high quality, repeatable data in the transverse imaging plane.

An ICC was evaluated to describe the reliability of the rater in repeatedly analyzing the same images. As mentioned, the reliability of the rater is distinct from the assessment of overall repeatability as it isolates image analysis whereas repeatability contains both imaging error and analysis error. By quantifying the image analysis error, we may better understand over repeatability. The 95% CI for the transverse imaging method was 0.554 to 0.650 which indicates moderate reliability (Koo and Li, 2016).

5.2   Robustness

Recall that robustness was defined as a measure of how naturally protected the measurement system is to human error. When carrying out the robustness protocol, the intention was to capture a misleading image by systematically tilting and translating the ultrasound transducer. For example, when imaging the L1-L2 vertebrae in the sagittal plane, it was conceivable to measure a slightly different contour of one or both SPs leading to a different spacing measurement. If it was difficult to make such an error, then the measurement system would be considered robust. Robustness was assessed by comparing the difference in SP spacings taken from ideal images (the images that are used to assess reliability) and non-ideal images (images with less distinct features but which are still measurable). Sagittal imaging robustness testing was conducted in two positions: neutral laying and laying in supported flexion.

A three-way mixed ANOVA (α = 0.05) was run to investigate the effect of sex (two levels, male and female), position (two levels, neutral and flexion), and repeat number (four levels) on image measurement differences. There were no significant within participant interactions ($F_{(3,108)}$ < 0.433, p > 0.729 or main effects ($F_{(3,108)}$ = 0.646, p = 0.587). There were no significant between participant interactions ($F_{(1,36)}$ = 1.004, p = 0.323) or main effects ($F_{(1,36)}$ < 2.165, p > 0.150). The 95% confidence interval for the overall mean (-0.266 to 0.051) demonstrates that difference between measurements is not statistically different from zero, and therefore the sagittal imaging method was considered robust to induced error.

The robustness of the sagittal imaging method was further supported by a Bland Altman difference plot which illustrated that 94.6% of the differences fall within 1.96 SDs of the mean (Figure 5.5). The measurement differences have a strong tendency towards zero and only rarely exhibit outliers.
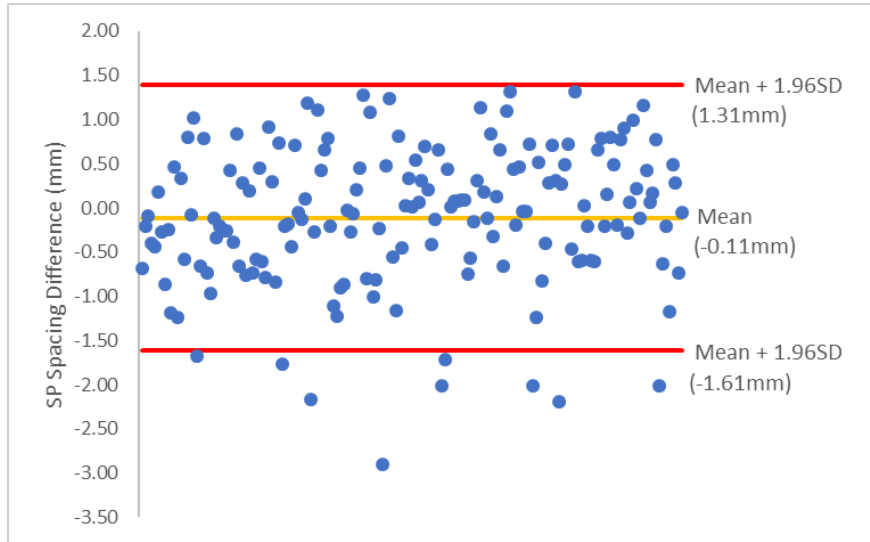
Figure 5.5 – Bland-Altman difference plot illustrating the distribution of measurement differences. 94.6% of data fell within 1.96SDs from the mean. Differences are obtained by subtracting the last measurable image from the ideal image measurement.

5.3   Image Acquisition Window

The imaging acquisition window describes the acceptable range of transducer movement during imaging in terms of tiling and translating. Within this window, a reliable image could be captured but beyond this window, the image deteriorated rapidly and could not be analyzed. This window was theorized based on in-vivo anatomical measurements and was tested here experimentally.

5.3.1 Sagittal Imaging

5.3.1.1 Sagittal Tilting Acquisition Window

A three-way ANOVA (α = 0.05) was conducted to compare the effects of participant sex (two levels; male and female), position (two levels; neutral and flexion), and direction of transducer tilt (two levels; left and right) on the size of the sagittal image acquisition window. No statistically significant interaction effects were found ($F_{(1,76)}$ < 3.157, p > 0.08). There was a statistically significant main effect for position $F_{(1,76)}$ = 4.482, p = 0.038) which suggests that the magnitude of tilting depends on the posture held by the participant. The tilting acquisition window was 7.9° (95% CI: 6.4 to 9.5°) in the neutral position and 10.2° (95% CI: 8.7 to 11.7°) in the flexion position (Figure 5.6).
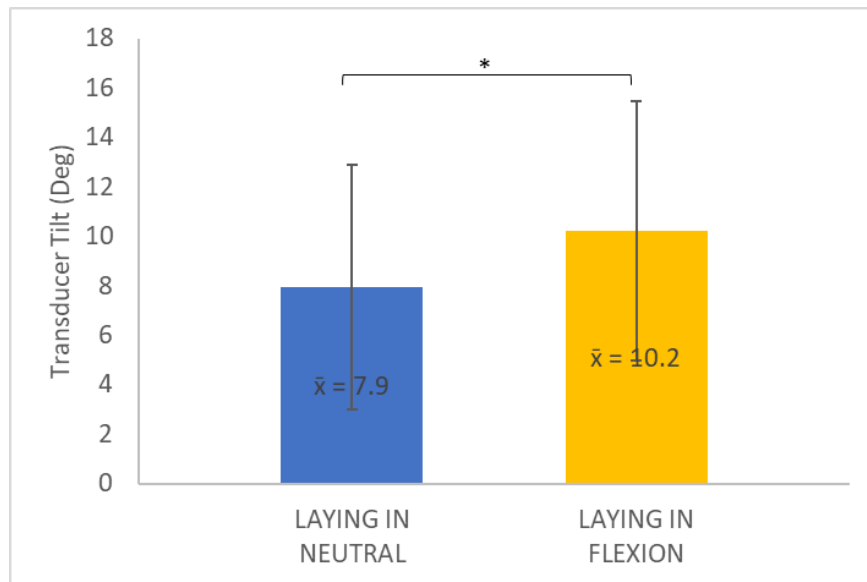
Figure 5.6 – The sagittal transducer tilting acquisition window (amount of transducer tilt in which reliable images can be captured) for both the neutral and flexion posture. A significant main effect was found for position ($F_{(1,76)}$ = 4.482, p = 0.038) therefore the windows are presented separately for each position.

5.3.2   Sagittal Translational Acquisition Window

A three-way ANOVA (α = 0.05) was conducted to compare the effects of participant sex (two levels), position (two levels), and direction of transducer translation (two levels) on the size of the sagittal image acquisition window. No statistically significant interaction effects ($F_{(1,68)} < 0.529$, $p > 0.469$) or main effects ($F_{(1,68)} < 3.492$, $p > 0.066$) were found. The tilting acquisition window was 4.0° on average (95% CI: 3.6 to 4.3°) (Figure 5.7).
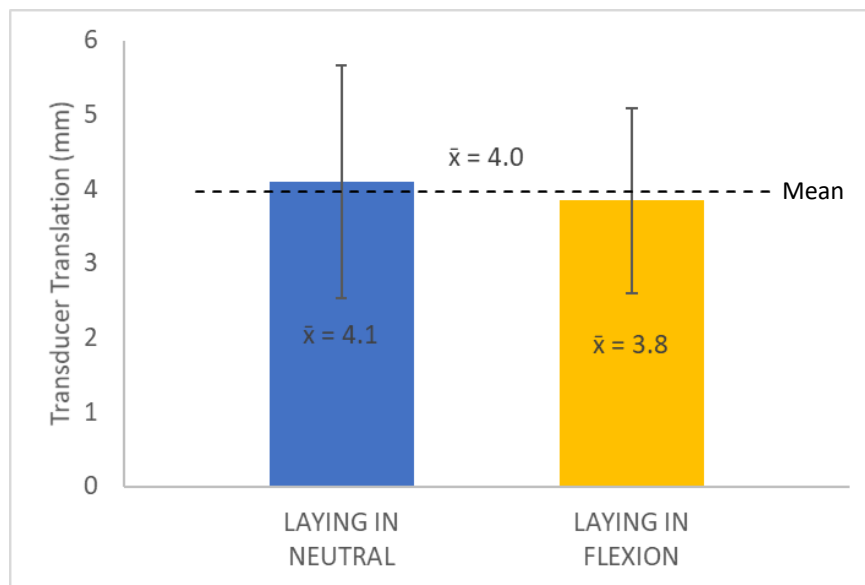
Figure 5.7 – Participant spine position did not affect the sagittal transducer translation image acquisition window (amount of transducer translation in which reliable images can be captured) $F_{(1,68)}$ < 3.492, p > 0.066. An average translation of 4.0mm about the mediolateral axis was observed.

5.3.3 Transverse Imaging

5.3.3.1 Transverse Tilting Acquisition Window

A three-way ANOVA (α = 0.05) was conducted to compare the effects of participant sex (two levels), position (two levels), and direction of transducer tilt (two levels) on the size of the transverse image acquisition window. No statistically significant interaction effects ($F_{(1,68)} < 1.696$, $p > 0.197$) or main effects ($F_{(1,68)} < 2.44$, $p > 0.123$) were found. The tilting acquisition window was 12.3° on average (95% CI: 11.3 to 13.3°) (Figure 5.8).
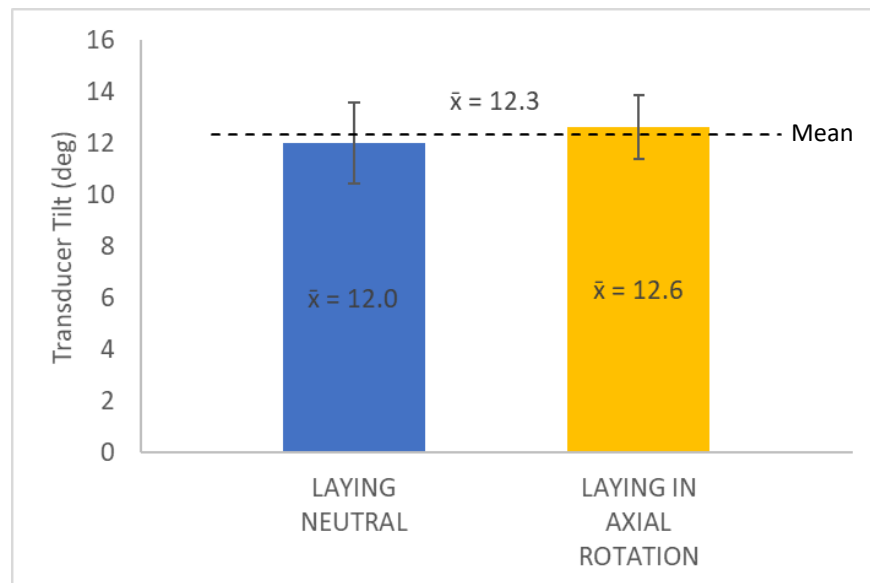
Figure 5.8 – Participant spine position did not affect the transverse transducer tilting image acquisition window (amount of transducer tilt in which reliable images can be captured) $F_{(1,68)} < 2.44$, $p > 0.123$. An average tilt of 12.3° about the mediolateral axis was observed.

5.3.3.2 Transverse Translational Acquisition Window

A three-way ANOVA (α = 0.05) was conducted to compare the effects of participant sex (two levels; male and female), position (two levels; neutral and axially rotated), and direction of transducer translation (two levels; superiorly and inferiorly) on the size of the transverse image acquisition window. No statistically significant interaction effects ($F_{(1,60)} < 1.208$, $p > 0.276$) or main effects ($F_{(1,60)} < 2.44$, $p > 0.124$) were found. The translation acquisition window was 7.6mm on average (95% CI: 6.7 to 8.6mm) (Figure 5.9).
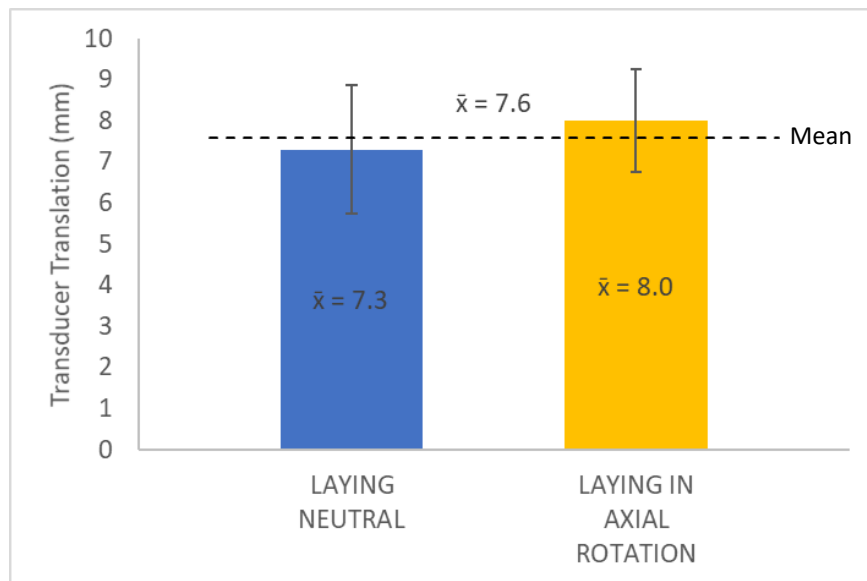
Figure 5.9 – Participant spine position did not affect the transverse transducer translation image acquisition window (amount of transducer translation in which reliable images can be captured) $F_{(1,60)}$ < 2.44, p > 0.124. An average translation of 7.6mm along the mediolateral axis was observed.

5.4   MMH Tasks

5.4.1   Flexion Results

The MMH tasks involved three standardized positions, each was held for approximately five minutes to allow synchronized ultrasound imaging and surface-based optoelectronic motion capture. Again, these three tasks were designed to elicit spine positions of predominant rotation (11 Series), mixed axial rotation and flexion (12 Series) and pure flexion (13 Series). The results of each task were presented below in the order they were completed, expressed in both relative and absolute terms. Relative ROM was calculated by expressing joint-level ROM to the participant's total ROM across all levels. This relative "percentage total" joint motion was important to consider as it highlighted the different movement profiles exhibited by various participants. The same data are then presented as absolute intervertebral joint ROM measured in millimeters of space between SPs for comparative purposes. Absolute spacing measures are vital in understanding the magnitude of any differences in movement patterns that may be observed.

For example, in the MMH flexion task, participant LAD displayed 48% of their lumbar flexion ROM at L2-L3 or stated in absolute terms, displayed 22mm of change in SP spacing at L2-L3 out of a total of 45mm across L1 through L5 for this task. Such a large amount of movement at one joint should be identified as is likely to strain passive structures and may increase risk of LBP. On the other hand, in this same task, participant ACS displays 62% of their total ROM at L2-L3, which may appear alarming in relative terms but when presented in absolute terms equates to just 5mm of change in SP spacing. In this case, despite the high percentage of joint ROM expressed at a singular joint, the absolute amount of motion expressed is not likely troublesome. Therefore, in order to ensure that important details are not overlooked, both absolute and relative measures were analyzed via box and whisker plots and the results were presented together. Both absolute and relative ROM were considered outliers if the ROM was beyond 1.5x the interquartile range.

In the flexion reference task, there were five outliers identified by relative measures and two identified by absolute measures (Figure 5.10 & Table 5.1). While some outliers were identified by absolute measures, it appears that understanding the distribution of joint motion through relative measures was fundamental in being able to fully characterize intervertebral movement. Further, no outliers were identified via boxplot for the absolute ROM totals which once again supports the need for analysis of each intervertebral joint. A graphical description of relative and absolute joint ROM for all participants is also provided (Figure 5.11 & Figure 5.12). These figures illustrate ultrasound's ability to identify outlier ROM.

Figure 5.10 – Box plot analysis for flexion reference task. Left: box plot of SP spacing relative measure for each participant at each vertebral level showing outlier ROM at L2-L3, L3-L4 and L4-L5. Right: box plot of SP spacing absolute measure for each participant at each vertebral level showing outlier ROM at L1-L2 and L3-L4, but no outliers for the sum-total across joints.

Table 5.1 – List of outliers identified by box and whisker plot (1.5 IQR) of relative and absolute measures in the flexion reference task. '#' denotes the source of the outlier (relative or absolute measure).

LEVEL & PARTICIPANT		RELATIVE MEASURE	ABSOLUTE MEASURE
L1-L2		MEAN 6.05%, MEDIAN 3.9%	MEAN 8.3mm, MEDIAN 6.2mm
	MDS	21.0%	22.21mm (#)
L2-L3		MEAN 11.4%, MEDIAN 12.0%	MEAN 7.7mm, MEDIAN 7.7mm
	JIM	20.5% (#)	6.2mm
L3-L4		MEAN 15.4%, MEDIAN 15.9%	MEAN 10.4mm, MEDIAN 11.2mm
	COP	9.0% (#)	5.6mm
	RAK	2.7% (#)	1.33mm (#)
	JIM	24.6% (#)	7.47mm
L4-L5		MEAN 14.9%, MEDIAN 15.0%	MEAN 10.6mm, MEDIAN 11.5mm
	BEN	38.6% (#)	11.78mm
TOTAL ACROSS LEVELS		n/a	MEAN 33.8mm, MEDIAN 32.5mm
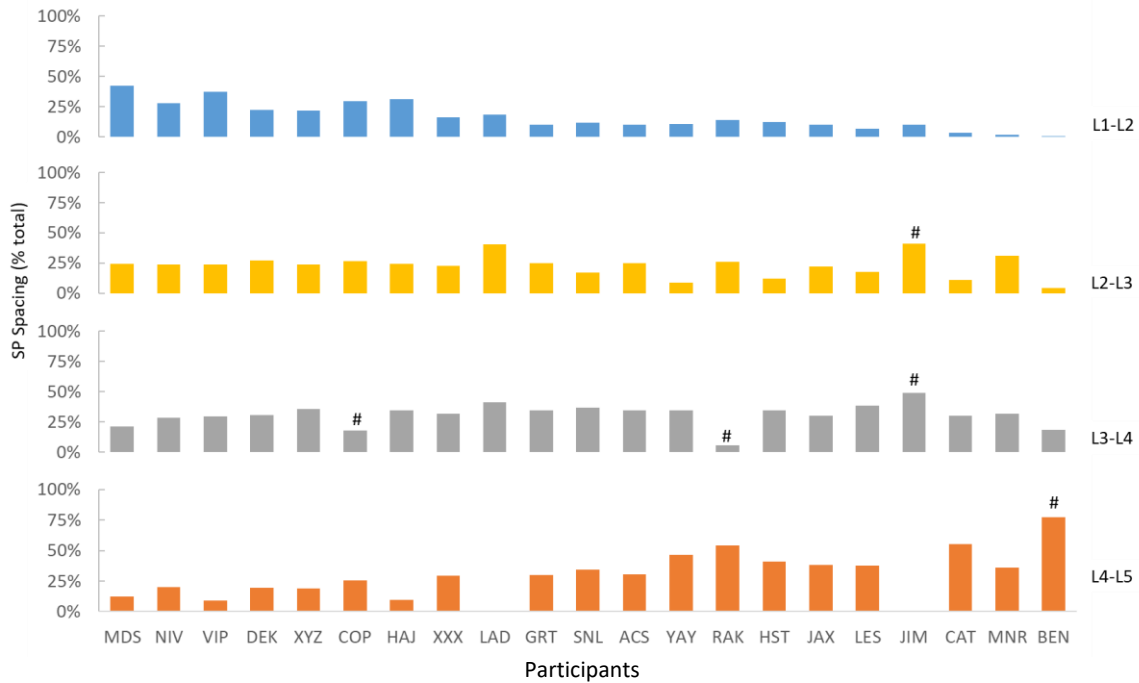
Figure 5.11 – Flexion reference test percentage ROM at each joint for each participant (%). Calculated as joint-level ROM relative to total ROM for each participant. '#' indicates an outlier identified by boxplot (value outside of 1.5x IQR).
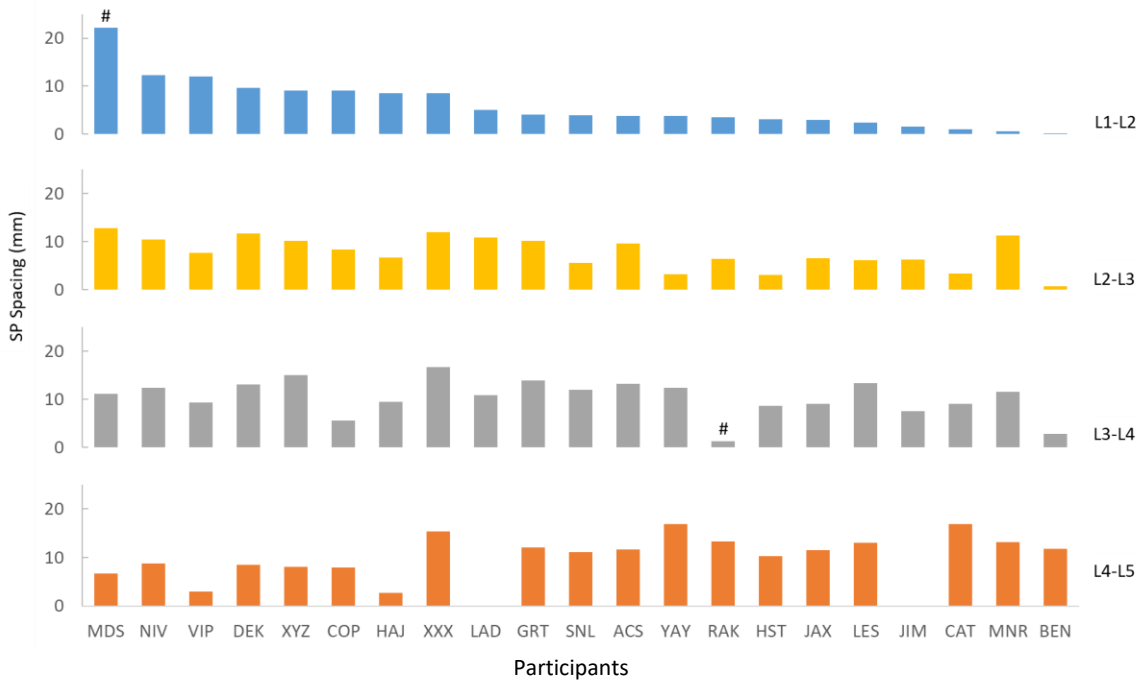
Figure 5.12 – Absolute ROM (mm) at each joint for the flexion reference test for each participant. '#' indicates an outlier identified by boxplot (value outside of 1.5x IQR).

In the MMH rotation task, there were two outliers identified from relative measures (% ROM), three identified by absolute measures (mm ROM), and two detected via absolute ROM totals (Figure 5.13 & Table 5.2). A graphical description of relative and absolute joint ROM for all participants is also provided (Figure 5.14 & Figure 5.15). Again, these figures demonstrate ultrasound's ability to detect outlier ROM.
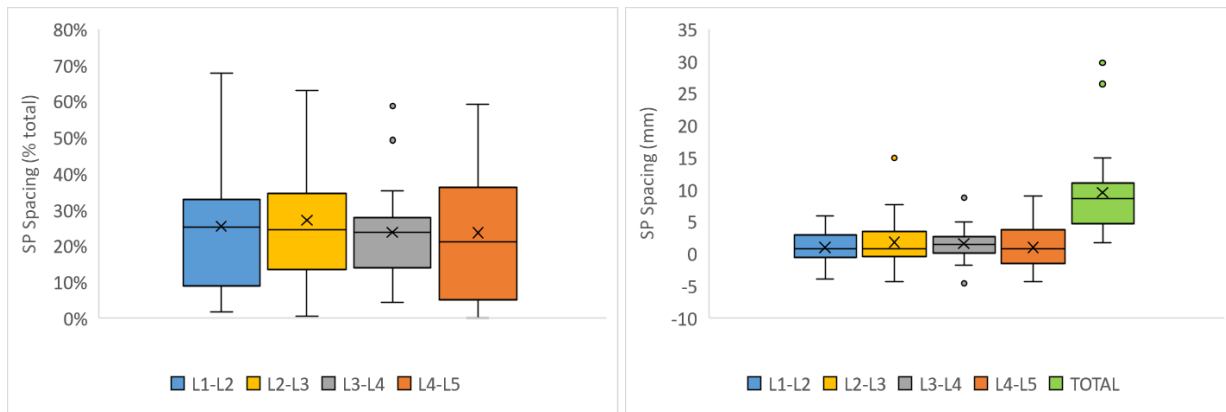
Figure 5.13 – Box plot analysis for MMH rotation task. Left: box plot of SP spacing relative measure for each participant at each vertebral level showing outlier ROM at L3-L4. Right: box plot of SP spacing absolute measure for each participant at each vertebral level showing outlier ROM at L2-L3, L3-L4, and for the sum-total across joints. Both plots depict intervertebral joint flexion during the MMH rotation task.

Table 5.2 - List of outliers identified by box and whisker plot (1.5 IQR) of relative and absolute measures in the MMH rotation task. '#' denotes the source of the outlier and '*' indicates that the participant's movement involved some quantity of extension.

LEVEL & PARTICIPANT		RELATIVE MEASURE	ABSOLUTE MEASURE
TOTAL ACROSS LEVELS		**n/a**	**MEAN 9.5mm, MEDIAN 8.6mm**
	LAD	n/a	29.8mm (#)
	MNR	n/a	26.4mm (#)
L1-L2		**MEAN 6.05%, MEDIAN 3.9%**	**MEAN 1.0mm, MEDIAN 0.8mm**
L2-L3		**MEAN 11.4%, MEDIAN 12.0%**	**MEAN 1.8mm, MEDIAN 0.8mm**
	LAD	50.1%	14.9mm (#)
L3-L4		**MEAN 15.4%, MEDIAN 15.9%**	**MEAN 1.5mm, MEDIAN 1.5mm**
	COP	49.2% (#)(*)	-4.62mm (#)
	RAK	58.9% (#)(*)	-1.56mm
	MNR	33%	8.72mm (#)
L4-L5		**MEAN 14.9%, MEDIAN 15.0%**	**MEAN 1.0mm, MEDIAN 0.7mm**
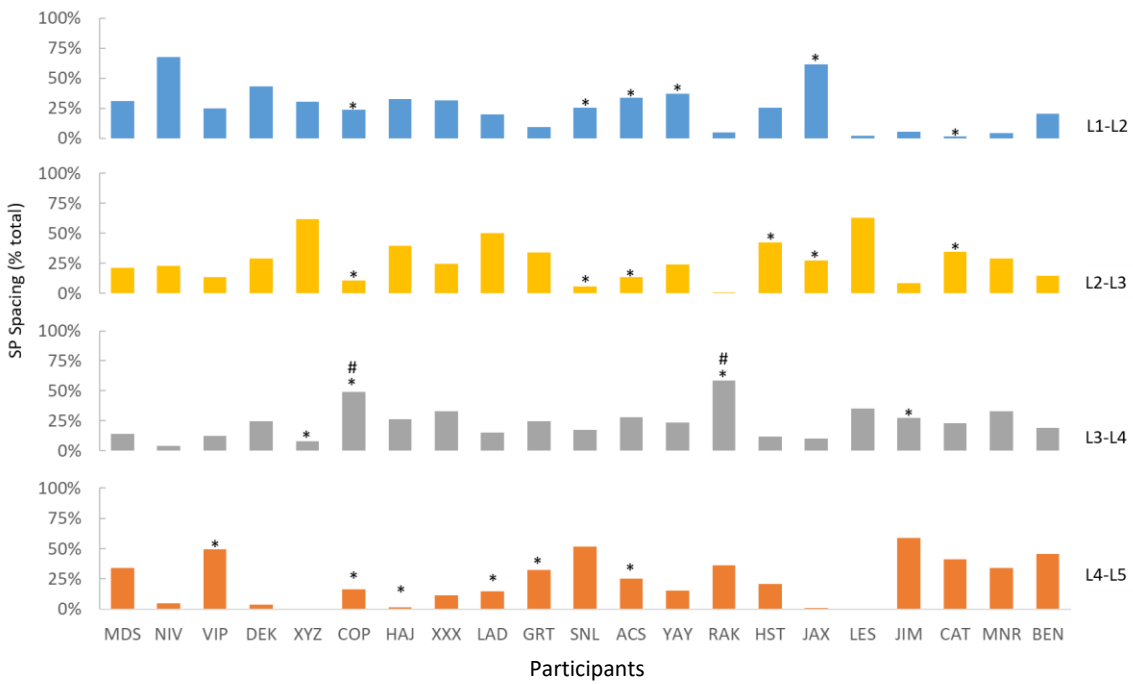
Figure 5.14 – MMH rotation task percentage ROM (%). Calculated as joint-level ROM relative to total ROM for each participant. '#' indicates an outlier identified by boxplot (value outside of 1.5x IQR). and '*' indicates that the participants movement involved some quantity of extension.
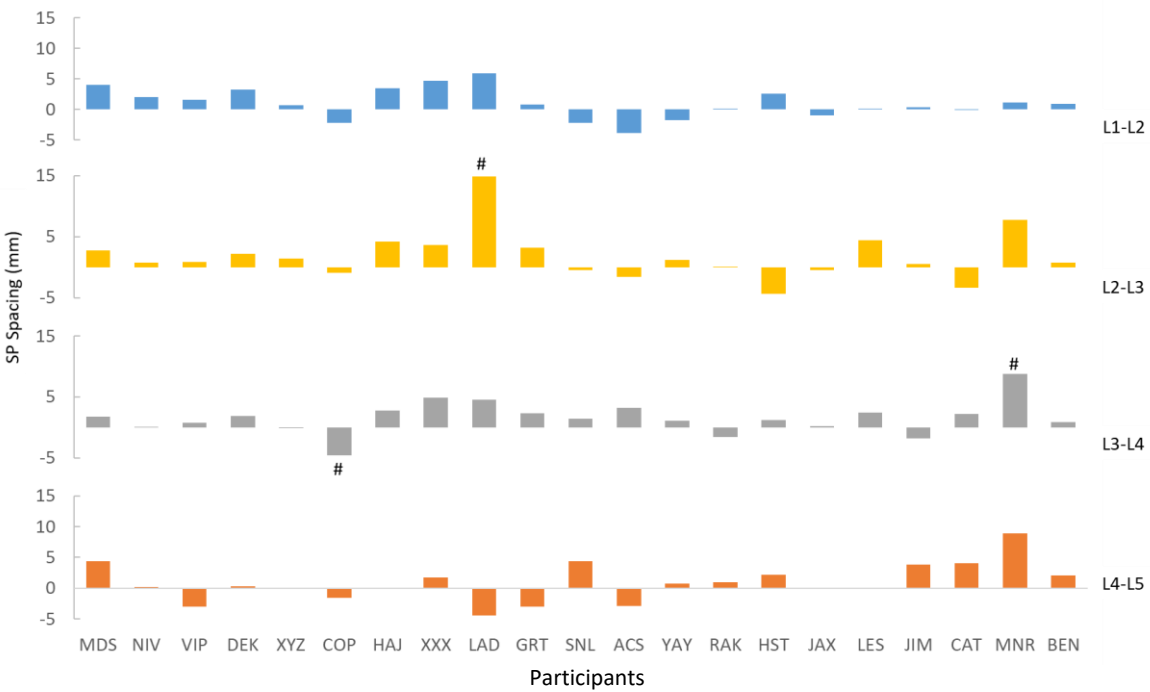
Figure 5.15 – MMH rotation task absolute ROM (mm). '#' indicates an outlier identified by boxplot (value outside of 1.5x IQR).

In the MMH mixed axial rotation and flexion task, two outliers were identified by relative measures and three outliers were identified by absolute measures (Figure 5.16 & Table 5.3). No outliers were detected within absolute ROM totals. A graphical description of relative and absolute joint ROM for all participants is also provided (Figure 5.17 & 5.18). Again, these figures demonstrate ultrasound's ability to detect outlier ROM.
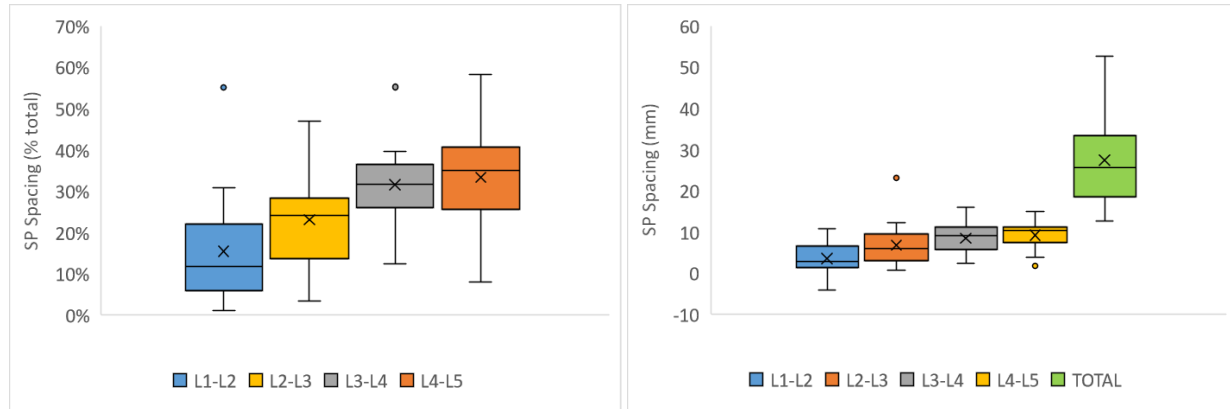
Figure 5.16 – Box plot analysis for MMH mixed axial rotation and flexion task. Left: box plot of SP spacing relative measure for each participant at each vertebral level showing outlier ROM at L1-L2 and L3-L4. Right: box plot of SP spacing absolute measure for each participant at each vertebral level showing outlier ROM L2-L3 and L4-L5, but no outliers for the sum-total across joints.

Table 5.3 - List of outliers identified by box and whisker plot (1.5 IQR) of relative and absolute measures in the MMH mixed axial rotation and flexion task. '#' denotes the source of the outlier and '$' indicates that the participant is missing data for L4-L5 ROM, which will distort relative measures.

LEVEL & PARTICIPANT		RELATIVE MEASURE	ABSOLUTE MEASURE
TOTAL ACROSS LEVELS		*n/a*	**MEAN 27.4mm, MEDIAN 25.6mm**
L1-L2		**MEAN 15.4%, MEDIAN 11.6%**	**MEAN 3.5mm, MEDIAN 2.7mm**
	NIV	55.2% (#)	10.63mm
L2-L3		**MEAN 23.0%, MEDIAN 24.0%**	**MEAN 6.7mm, MEDIAN 6.0mm**
	LAD	46.1%	23.1mm (#)
L3-L4		**MEAN 31.5%, MEDIAN 31.6%**	**MEAN 8.4mm, MEDIAN 9.0mm**
	JIM	55.2% (#)($)	7.94mm
L4-L5		**MEAN 33.3%, MEDIAN 35.0%**	**MEAN 9.1mm, MEDIAN 10.2mm**
	NIV	9.0%	1.74mm (#)
	VIP	8.0%	1.91mm (#)
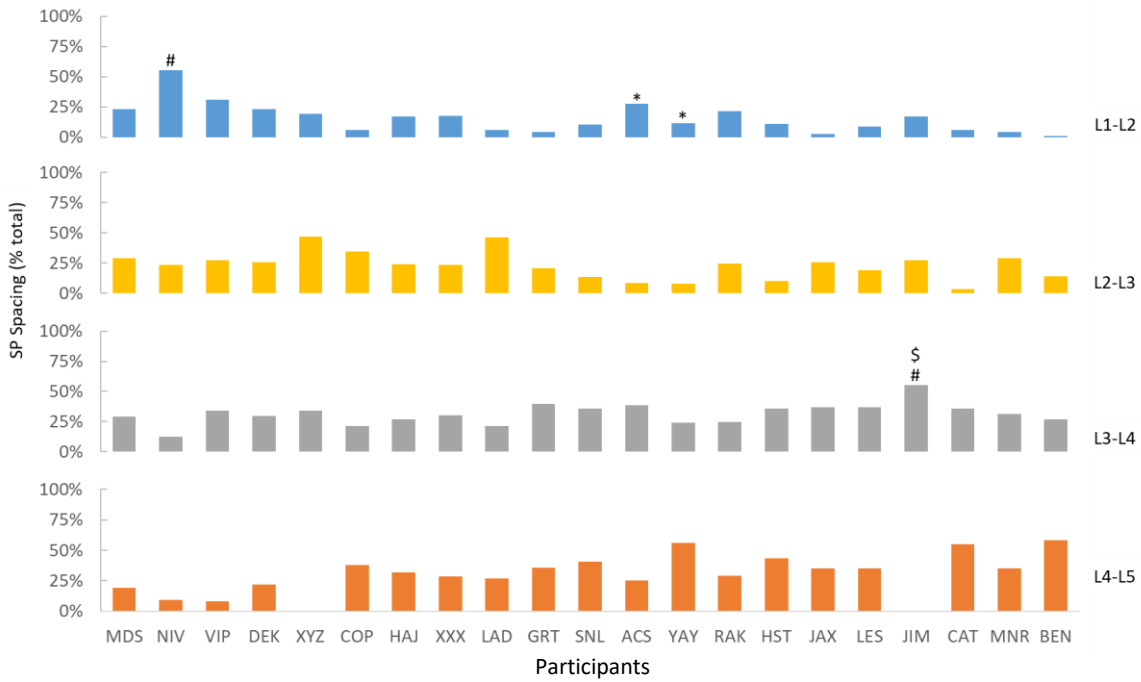
Figure 5.17 – MMH mixed axial rotation and flexion task percentage ROM (%). Calculated as joint-level ROM relative to total ROM for each participant. '#' indicates an outlier identified by boxplot (value outside of 1.5x IQR) and '*' indicates that the participants movement involved some quantity of extension. '$' indicates that the participant is missing L4-L5 ROM data which will skew proportions and the interpretation of the outlier.
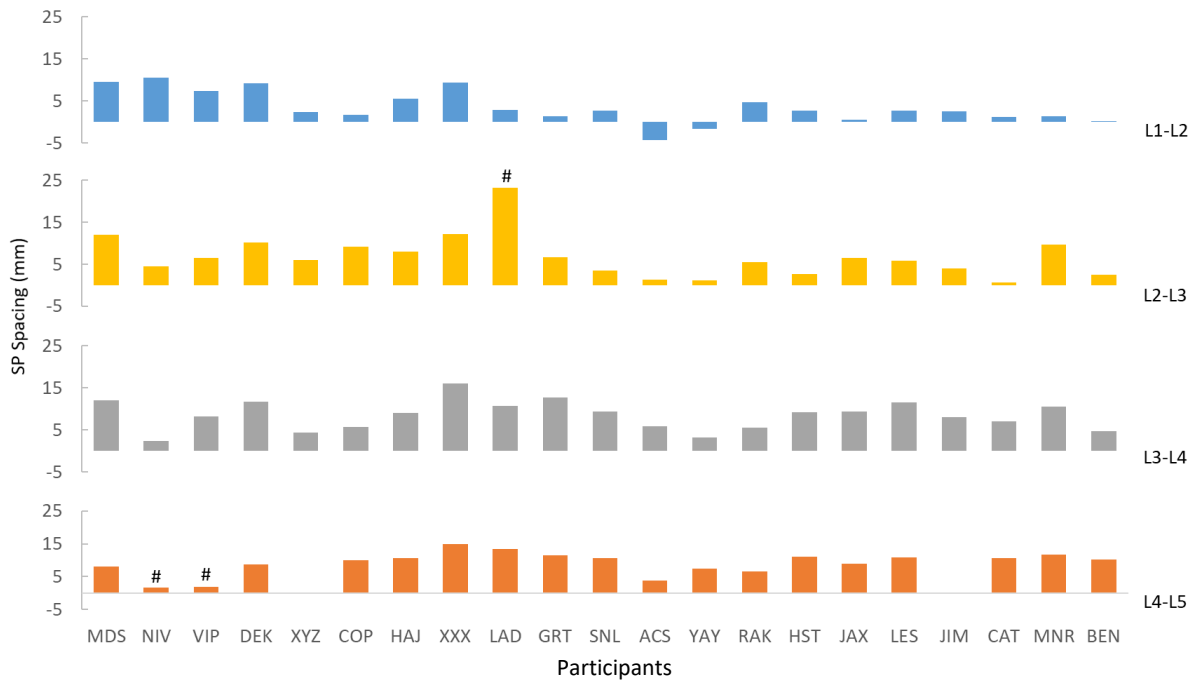
Figure 5.18 – MMH mixed axial rotation and flexion task absolute ROM (mm). Calculated as absolute joint-level measure relative to total absolute motion for each participant. '#' indicates an outlier identified by boxplot (value outside of 1.5x IQR).

In the MMH flexion task, five outliers were identified by relative measures and one was identified by absolute measures (Figure 5.19 & Table 5.4). No outliers were detected within absolute ROM totals. A graphical description of relative and absolute joint ROM for all participants is also provided (Figure 5.20 & 5.21). Again, these figures demonstrate ultrasound's ability to detect outlier ROM.
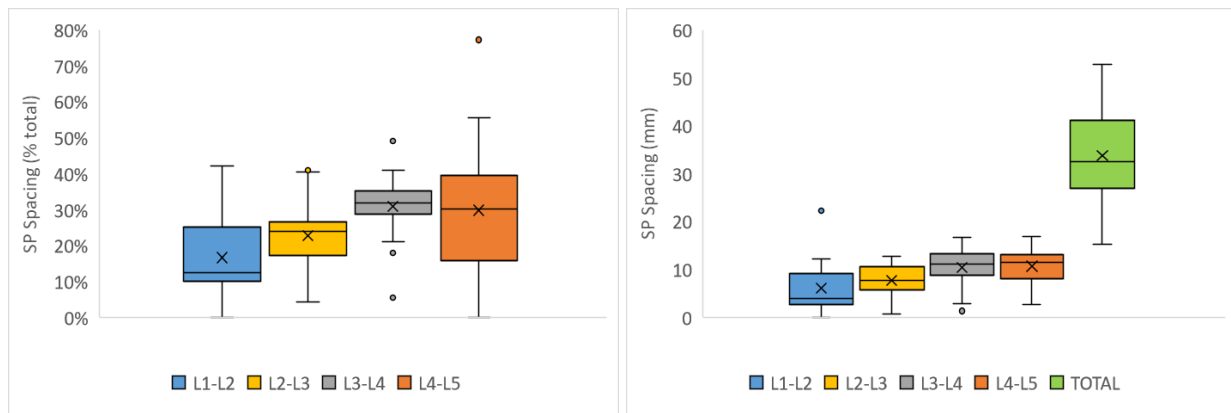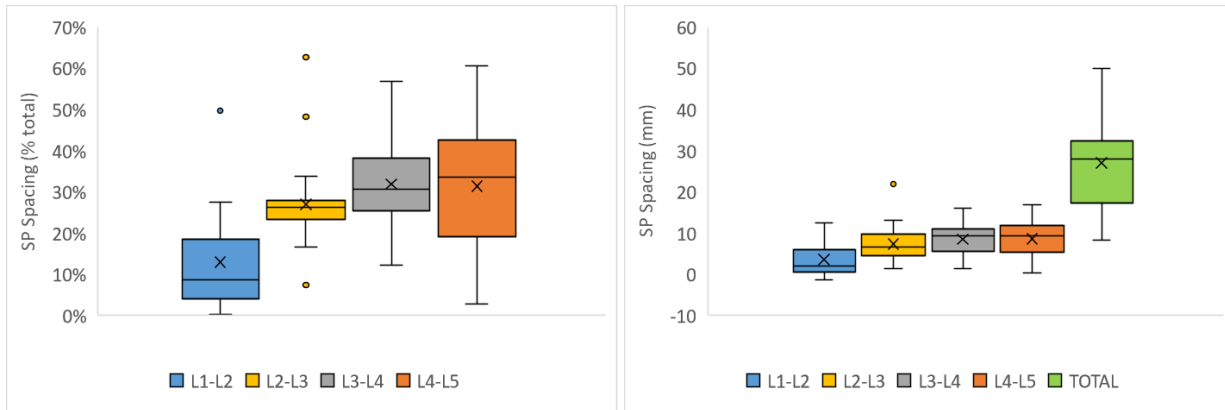

Figure 5.19 – Box plot analysis for MMH flexion task. Left: box plot of SP spacing relative measure for each participant at each vertebral level showing outlier ROM at L1-L2 and L2-L3. Right: box plot of SP spacing absolute measure for each participant at each vertebral level showing outlier ROM at L1-L2, but no outliers for the sum-total across joints. Both plots depict intervertebral joint flexion during the MMH flexion task.

Table 5.4 - List of outliers identified by box and whisker plot (1.5 IQR) of relative and absolute measures in the MMH flexion task. '#' denotes the source of the outlier.

LEVEL & PARTICIPANT		RELATIVE MEASURE	ABSOLUTE MEASURE
TOTAL ACROSS LEVELS		**n/a**	**MEAN 27.0mm, MEDIAN 27.8mm**
L1-L2		**MEAN 12.9%, MEDIAN 8.6%**	**MEAN 3.5mm, MEDIAN 1.9mm**
	NIV	49.7% (#)	12.44mm
L2-L3		**MEAN 26.9%, MEDIAN 26.2%**	**MEAN 7.2mm, MEDIAN 6.5mm**
	LAD	48.2% (#)	21.8mm (#)
	SNL	8.4% (#)	1.2mm
	ACS	62.7% (#)	5.8mm
	CAT	7.3% (#)	2.1mm
L3-L4		**MEAN 31.9%, MEDIAN 30.6%**	**MEAN 8.4mm, MEDIAN 9.2mm**
L4-L5		**MEAN 31.3%, MEDIAN 33.5%**	**MEAN 8.5mm, MEDIAN 9.3mm**
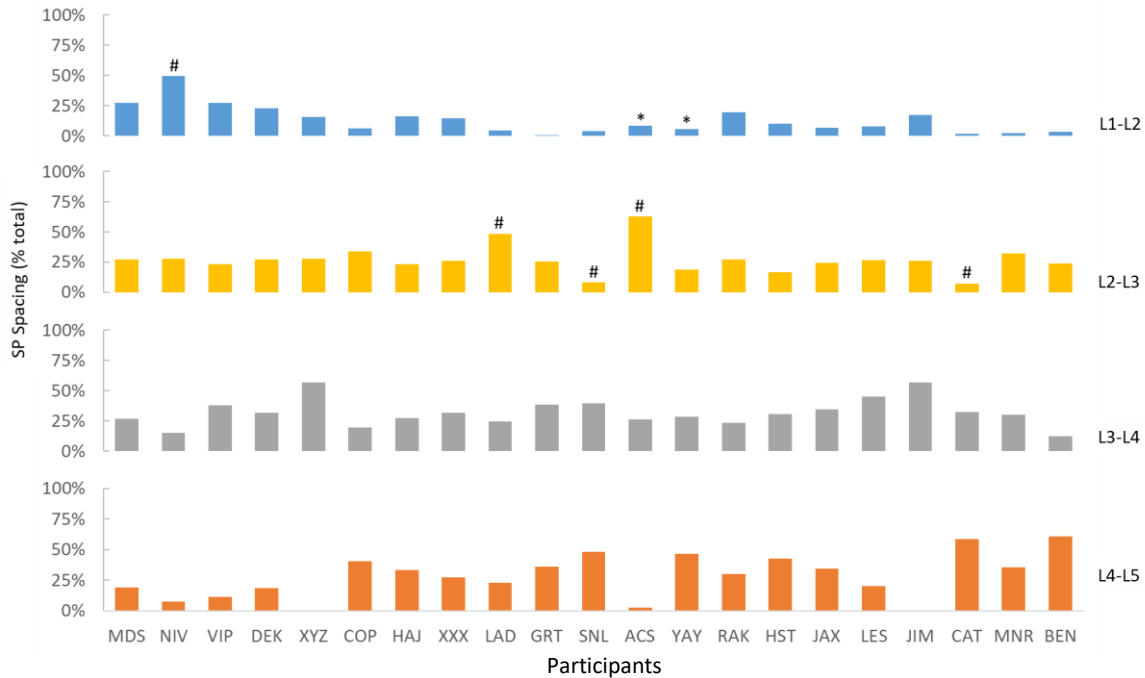
Figure 5.20 – MMH flexion task percentage ROM (%). Calculated as joint-level ROM relative to total ROM for each participant. '#' indicates an outlier identified by boxplot (value outside of 1.5x IQR) and '*' indicates that the participants movement involved some quantity of extension.
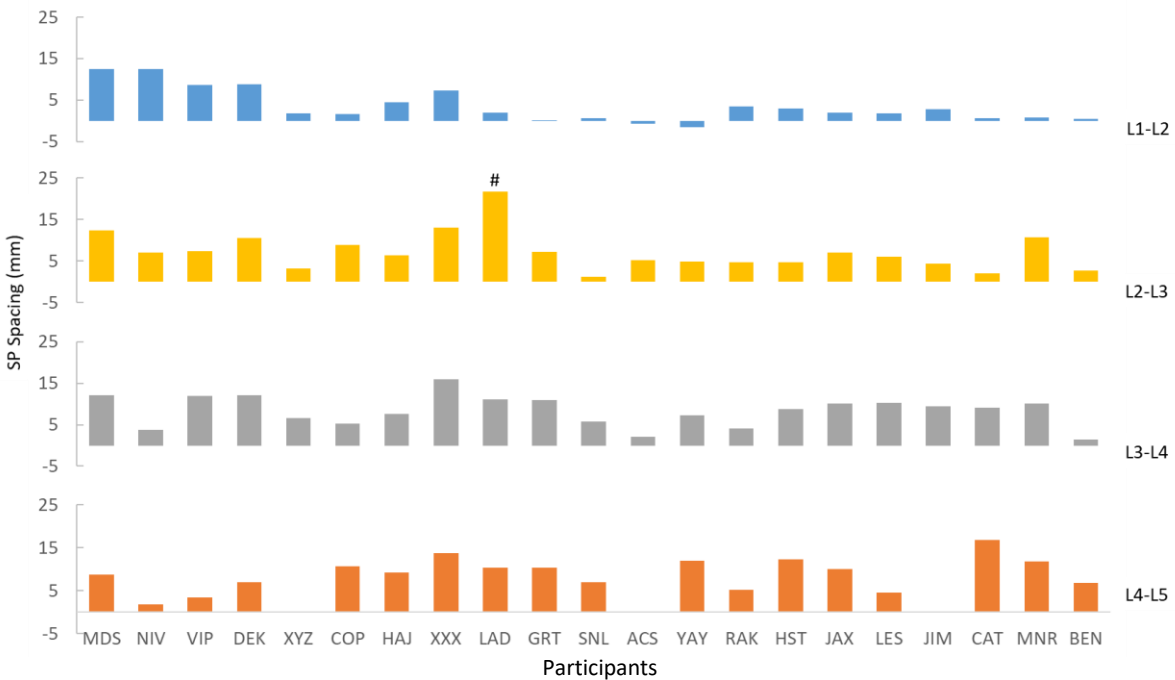
Figure 5.21 – MMH flexion task absolute ROM (mm). Calculated as absolute joint-level measure relative to total absolute motion for each participant. '#' indicates an outlier identified by boxplot (value outside of 1.5x IQR).

The preceding analysis of joint-level relative and absolute ROM highlighted discrepant ROM in several participants across the various tasks. In total, there were 14 outliers identified by relative measures and nine outliers identified by absolute measures, in the flexion reference task and the three MMH tasks (Table 5.2, Table 5.3, and Table 5.4). A similar analysis of the surface-based optoelectronic motion capture data during the same tasks revealed only one outlier, discovered in the MMH mixed axial rotation and flexion task (Figure 5.22). These findings suggest that ultrasound-based measurement of lumbar flexion was able to identify movement irregularities which were not captured by surface-based optoelectronic motion capture.
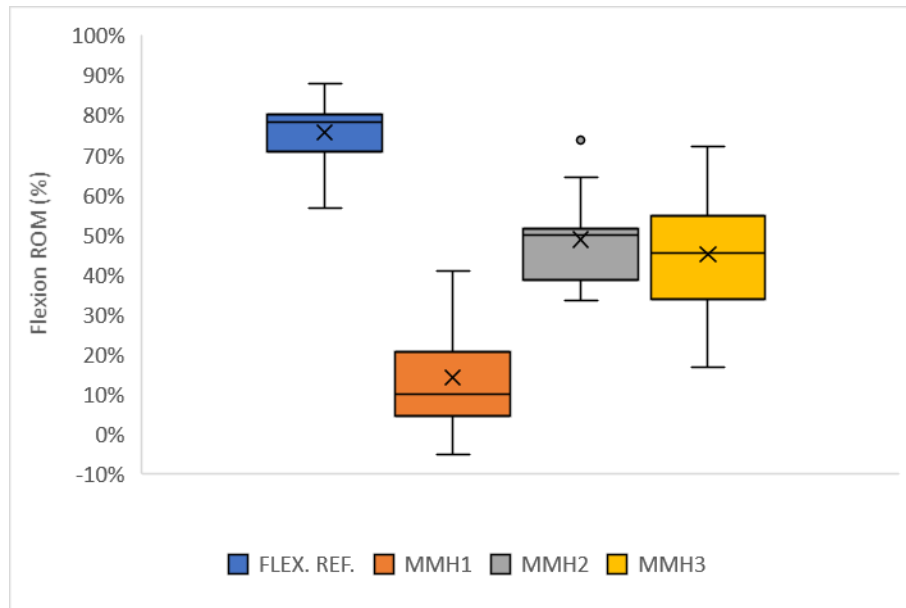
Figure 5.22 – Box plot of flexion ROM during the flexion reference task and the three MMH tasks (MMH1: lumbar axial rotation, MMH2: mixed lumbar axial rotation and flexion, and MMH3: lumbar flexion) in the subgroup of 10 participants demonstrating the detecting of only one outlier from surface-based motion capture data. Data are expressed relative to the maximum flexion position.

5.4.2 Axial Rotation Results

As mentioned previously, the MMH tasks involved three standardized postures, each held for roughly five minutes to allow synchronized ultrasound imaging and surface-based optoelectronic motion capture. The three tasks were meant to encourage positions of predominant rotation (11 Series), mixed axial rotation and flexion (12 Series), and predominant flexion (13 Series). Transverse standing neutral imaging was done prior to the MMH tasks to quantify the relationship between the transducer and the sacrum rigid body in a neutral posture. The results presented here were relative to this neutral posture, i.e. they represent the change in orientation of the vertebrae about the longitudinal axis of the pelvis constructed in Visual3D.

A statistical approach was first applied to test for differences in the ultrasound method versus surface-based optoelectronic motion capture for the 10 participants with additional L1-S1 motion capture data. A two-way ANOVA ($\alpha = 0.05$) was conducted to compare the effects of participant sex (two levels), task (three levels) on the difference between ultrasound and surface-based optoelectronic motion capture measures of axial rotation within the L1-S1 region. No statistically significant interaction effect ($F_{(2,24)} = 0.047$, p = 0.954) was found however a main effect for sex was found ($F_{(1,24)} = 8.66$, p = 0.007). The difference between ultrasound and surface-based optoelectronic motion capture axial rotation measures were (95% CI) -0.18° to 4.62° in females and (95% CI) -6.14° to -0.25° in males across the three MMH tasks. The male confidence interval did not contain zero and therefore there was a statistically significant difference between ultrasound and optoelectronic measurements.

A graphical representation can also be helpful to understand similarities and discrepancies between ultrasound and optoelectronic motion capture. Presented first was the MMH pure rotation task (Figure 5.23), followed by MMH mixed axial rotation and flexion (Figure 5.25) and lastly the MMH flexion task (Figure 5.27). Participant JIM was removed from this part of the analysis due to missing data.
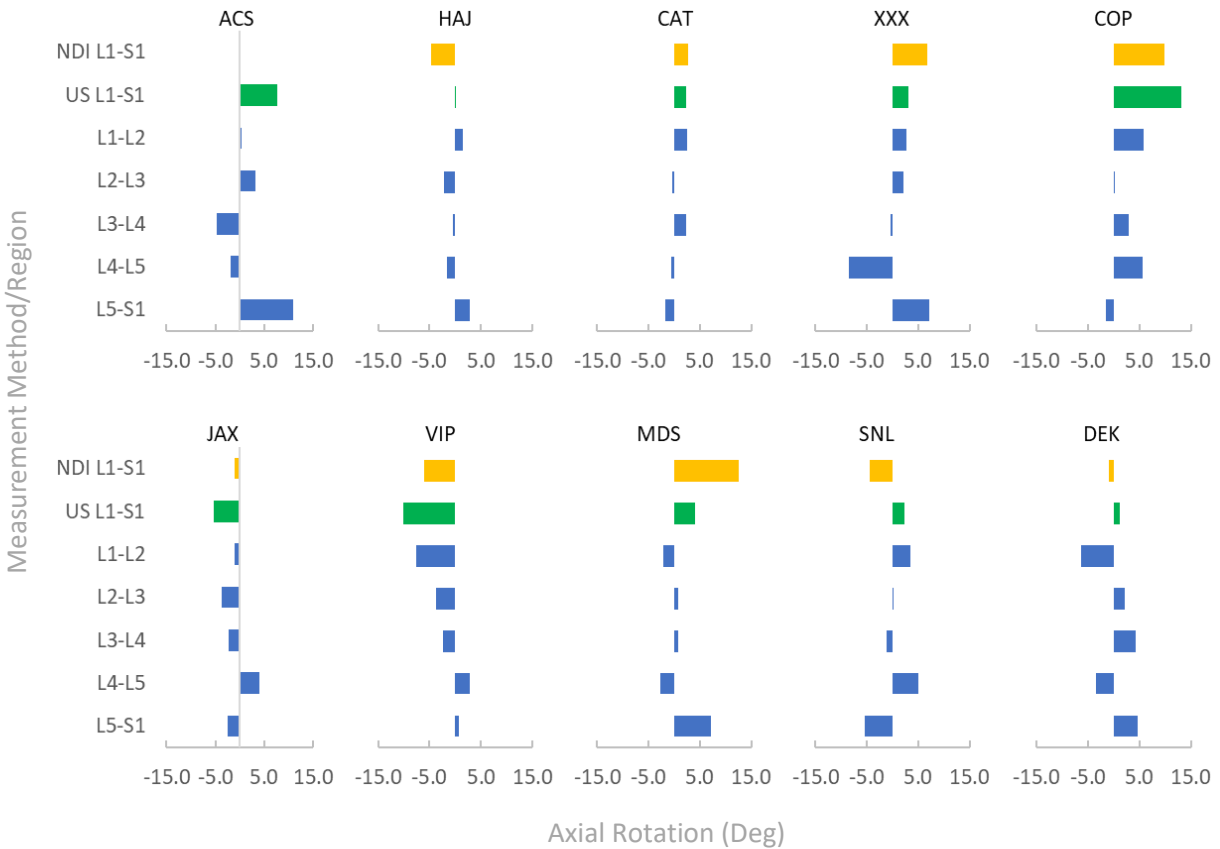
Figure 5.23 – Axial rotation measurement in MMH rotation task. Dark orange represents spine axial rotation measured by surface-based optoelectronic motion capture from T10 down to S1 and yellow represents axial rotation measured by surface-based optoelectronic motion capture from L1 down to S1 (only measured in a subset of n=10). Green represents the sum-total of ultrasound axial rotation measurements (individual measurements in blue).

For the MMH rotation task (Figure 5.23), the difference between optoelectronic L1-S1 axial rotation and the ultrasound sum-total was within 2° or less in only one of 10 participants (participant DEK) (Figure 5.24). The remaining nine of 10 participants had sum-total ultrasound measurements which differed from surface-based optoelectronic motion capture by more than 2° in either direction. Five of 10 participants had sum-total ultrasound measurements which were larger than surface-based optoelectronic motion capture (the negative differences observed in Figure 5.23) and four of 10 had sum-total ultrasound measurements which were less than surface-based motion capture. According to published norms for in-vivo axial rotation of the lumbar spine (Fujii et al., 2007; White and Panjabi, 1978),

error beyond 2° would be enough to obscure the ROM of one entire intervertebral joint and therefore the transverse method does not appear to provide any addition resolution over surface-based motion capture in the task of predominant rotation.
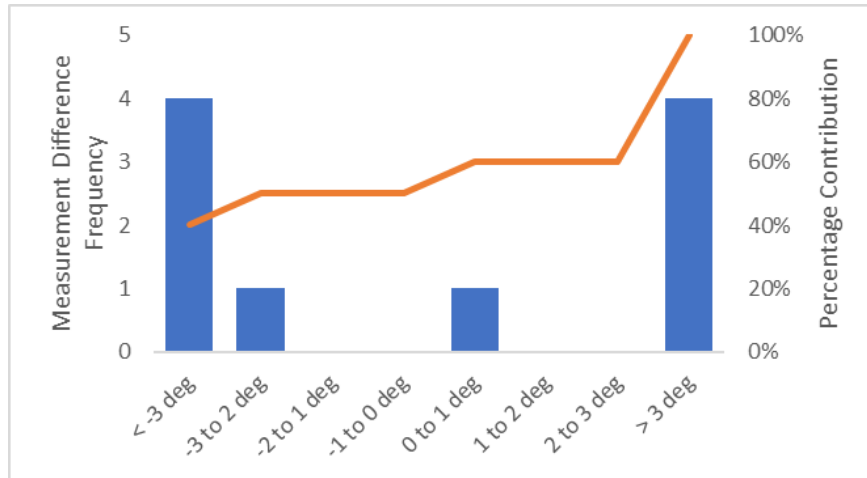
Figure 5.24 – Frequency of measurement differences between surface-based optoelectronic motion capture measured with the L1-S1 rigid body vs the sum-total of ultrasound axial rotation measurements during the MMH rotation task. Percentage contribution of each frequency bin shown at right. One participant had acceptable values with <2° discrepancy. A negative difference indicates that the ultrasound sum-total measurements were greater than those measured by surface-based optoelectronic motion capture.

The results for the MMH mixed axial rotation and flexion task were presented next (Figure 5.25). The difference between optoelectronic L1-S1 axial rotation and the ultrasound sum-total was within 2° or less in four of 10 participants (Figure 5.26). While the mixed axial rotation and flexion results are an improvement over the results for the axial rotation task, this amount of error was still unacceptable in six of ten participants since lumbar axial rotation ROM is typically less than 2° at each joint.
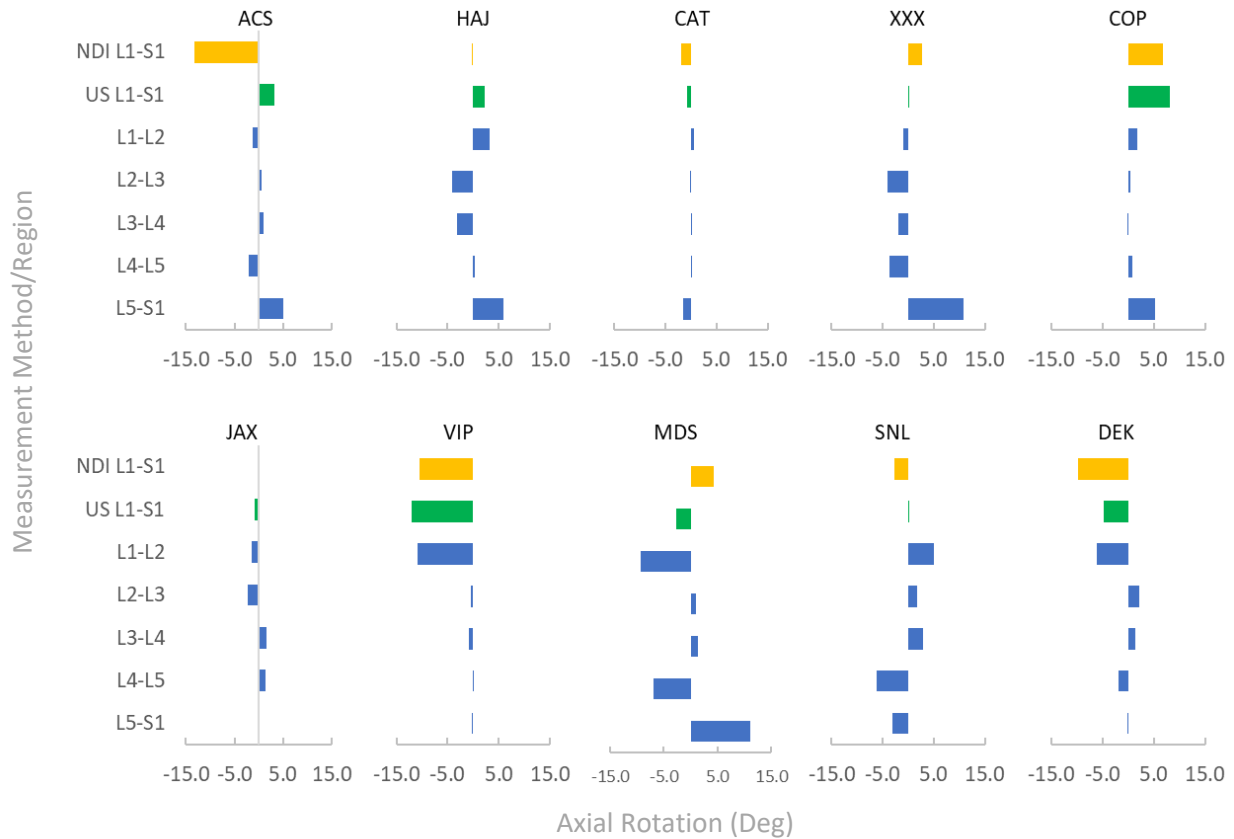
Figure 5.25 – Axial rotation measurement in the MMH mixed axial rotation and flexion task. Dark orange represents axial rotation measured by NDI from T10 down to S1 and yellow represents axial rotation measured by NDI from L1 down to S1 (only measured in a subset of n=10). Green represents the sum-total of ultrasound axial rotation measurements (individual measurements in blue).
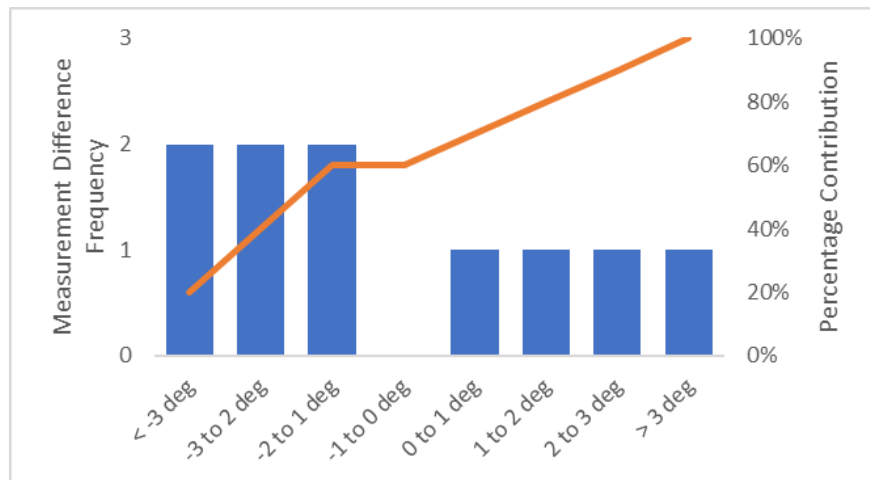
Figure 5.26 - Frequency of measurement differences between surface-based optoelectronic motion capture measured with the L1-S1 rigid body vs the sum-total of ultrasound axial rotation measurements in the MMH mixed axial rotation and flexion task. Percentage contribution of each frequency bin shown at right. Four participants had acceptable values with <2°discrepancy.

Lastly, for the MMH flexion task (Figure 5.27), the difference between surface-based optoelectronic L1-S1 axial rotation and the ultrasound sum-total was within 2° or less in three participants (Figure 5.28). Since 2° was shown to be a maximal rotation ROM in a single lumbar intervertebral joint, performance was likely insufficient in seven of ten participants. While these absolute amounts of error may be acceptable in other planes of motion, the limited axial rotation ROM of the lumbar spine reduces the tolerable measurement error. It should also be noted that while optoelectronic motion capture is often taken as the gold standard for external motion capture, there are long standing issues with measuring certain planes of motion, namely axial rotation. This fact was taken into consideration within the interpretation of results.
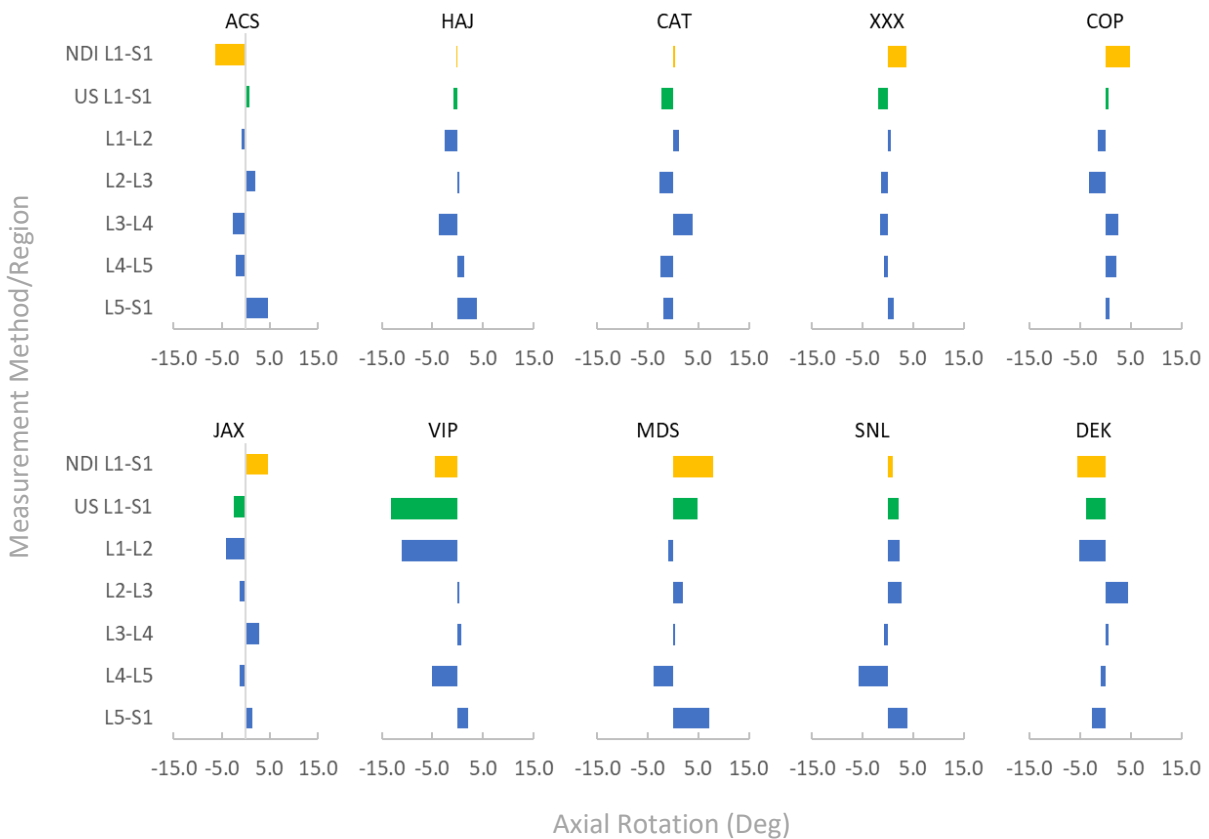
Figure 5.27 – Axial rotation measurement in the MMH flexion task. Dark orange represents spine axial rotation measured by NDI from T10 down to S1 and yellow represents axial rotation measured by NDI from L1 down to S1 (only measured in a subset of n=10). Green represents the sum-total of ultrasound axial rotation measurements (individual measurements in blue).
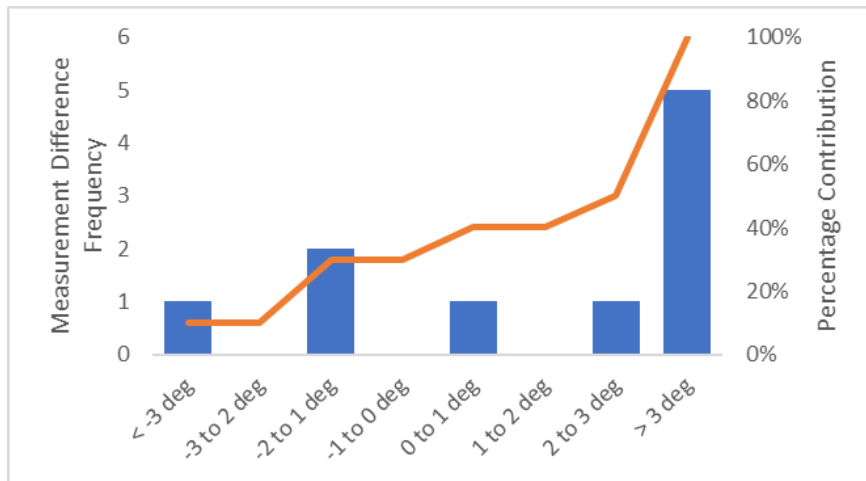
Figure 5.28 – Frequency of measurement differences between surface-based optoelectronic motion capture measured with the L1-S1 rigid body vs the sum-total of ultrasound axial rotation measurements in the MMH flexion task. Percentage contribution of each frequency bin shown at right. Three participants had acceptable values with <2° discrepancy. A negative difference indicates that the ultrasound sum-total measurements were greater than optoelectronic.

6   DISCUSSION

This study was the first to measure multiplanar intervertebral motions of the lumbar spine with ultrasound. The sagittal imaging method, which measured lumbar flexion movements was found to be repeatable, robust and capable of detecting abnormal ROMs which were not detected by surface-based optoelectronic motion capture. The transverse imaging method, which measured axial rotation was found to be repeatable in males, and appears to be acceptable in females if a standard imaging time between repeats and/or if only one image was captured (to alleviate the positive time-magnitude response possibly due to effects of creep in held imaging postures).

6.1   Hypotheses Revisited

The hypotheses from section 2.3 were reproduced here and are discussed below.

1. **Repeatability**

    a. *There will be a difference in ideal images within participants, within positions measured via SP spacing (i.e. not repeatable).*

       Rejected. The three-way mixed ANOVA failed to show a significant difference between ideal image repeats and therefore, the sagittal imaging method was determined to be repeatable.

    b. *There will be a difference in ideal image axial rotation measurements within participants, within positions (i.e. not repeatable).*

       Failed to reject. The three-way mixed ANOVA and post hoc testing detected a significant difference between ideal image repeats one and two, one and three, and one and four in females. Therefore, the transverse imaging method was not determined to be repeatable across four repeats in females. There was a consistent increase in the magnitude of measurements with time in females. Therefore, it is likely that using a controlled image acquisition duration would be of benefit when collecting data from females.

2. **Robustness:** *There will be a difference between SP spacing measurements taken from ideal and non-ideal images (i.e. robust).*

    Reject. The three-way mixed ANOVA failed to show a difference between ideal and non ideal images indicating that the sagittal measurement system was considered robust.

3. **Transverse orientation acquisition window:** *On average, transverse images will tolerate a 20° tilt or less, bidirectionally about the mediolateral axis.*

   Failed to reject. The tilting window was found to be 12.3° on average across participants and positions about the mediolateral axis which was within the hypothesized window of 20° or less.

4. **Sagittal plane acquisition window:** *On average, sagittal images will tolerate a 14° tilt or less, bidirectionally about the longitudinal axis.*

   Failed to reject. The three-way ANOVA detected a significant difference in the tilting window between the neutral (7.9°) and flexion positions (10.2°) however both windows were within the hypothesized window of less than 14°.

5. **Accuracy of intervertebral motion**

   a. *Ultrasound will not identify additional outlier ROM when compared to surface-based regional motion capture.*

      Rejected. In the flexion reference task and the three MMH tasks, only one outlier was identified via regional motion capture whereas 14 outliers were detected via ultrasound relative measures. This suggests that differences in joint level relative ROM were detected by ultrasound.

   b. *There will be a significant difference in axial rotation calculated by ultrasound compared to regional motion capture.*

      Failed to reject. There was no significant difference in ultrasound-based axial rotation measurement compared to surface-based optoelectronic motion capture measures in females across the three MMH tasks however a significant difference was detected in males.

6.2   Interpretation

6.2.1   Sagittal Imaging

The sagittal imaging method was determined to be repeatable by comparison of repeated ideal images. Spinous processes, which were the only target in sagittal images, were close to the skin surface and therefore images contained limited noise from surrounding soft tissues. Robustness was also evaluated in the sagittal imaging method and no differences were found between ideal and non-ideal images. Taken together, these findings suggested that ideal images were repeatably captured and

analyzed without concern for capturing a misleading image. Sagittal imaging appeared to behave analogously to a binary signal having only two possible levels: ideal image or no image.

In 2012, Chleboun et al. compared ultrasound to MRI in its ability to measure relative changes between vertebrae in various degrees of flexion and extension, similar to the sagittal imaging method applied in this study. The researchers imaged L1-L2, L2-L3, L3-L4 and L4-L5 in three separate positions, neutral, flexion and extension, yielding 12 total comparisons between ultrasound and MR imaging. While MRI and ultrasound analyses both showed strong interclass correlations (0.98 and 0.94), the researchers did find a statistically significant difference in ultrasound versus MRI measures when comparing flexion to the extended position at the L3-L4 joint. However, in the 11 remaining imaging pairs, MRI and ultrasound were not found to have any statistically significant differences. The MRI validation work presented by Chleboun et al. (2012) could not be directly compared to findings of this thesis, but their work indirectly supported the repeatability and robustness of the sagittal imaging method.

The sagittal imaging results of this thesis also agreed with the indirect findings of van den Hoorn et al. (2016). Briefly, van den Hoorn and colleagues (2016) described two techniques to measure lumbosacral motion. In the first part of their study, the two different techniques were validated in-vitro against a digital camera. The first technique involved mapping two points (and then lines) onto the surface of the sacrum and the superior vertebral body so that relative rotation could be determined. The second technique involved measuring linear spacing between only two points, and measurements were then related back to data captured with the first technique to establish relative rotation of the two rigid bodies. In the second part of the same study, van den Hoorn and colleagues compared both of their methods to fluoroscopy in anesthetized pig where they found it difficult to register two points on each vertebral body. The results of this thesis agreed with these indirect findings and were a preliminary motivation for tracking single points on SPs as done in Chleboun et al. (2012), instead of multiple points across laminae at oblique angles. While the in-vitro methods of van den Hoorn et al. (2016) had the advantage of presenting results

as degrees rotation instead of millimeter spacing, the method did not fare well in-vivo due to difficulty in imaging several points on each rigid body.

The sagittal imaging method using relative measures identified 14 outliers in the four measured tasks (flexion reference task, MMH rotation, MMH mixed axial rotation and flexion, and MMH flexion) while surface-based optoelectronic motion capture revealed only one outlier in the same tasks. While only one image was acquired at each intervertebral level in the MMH tasks, again the repeatability findings for the sagittal method suggest that this was adequate. In addition, many of the outlier ROMs expressed by a given participant were corroborated by other tasks demonstrating outlier ROM at the same intervertebral level. The ability to measure intervertebral joint motion demonstrated a clear advantage in being able to uncover abnormal ROM (either excessive or insufficient) which would not likely be discovered by surface-based optoelectronic motion capture.

6.2.2   Transverse Imaging

Repeatability in the transverse imaging method, which was assessed by comparing repeated ideal images, was determined to be repeatable only in males across four repeats. In females, there appeared to be a consistent increase in measurements across time suggesting that a controlled imaging duration may improve repeatability. Transverse images targeted both the spinous process and the laminae which are deep anatomical landmarks and were likely affected by proportionally more noise than sagittal plane images which targeted only the spinous processes. The depth of the landmarks (approximately 3 to 5cm) was likely responsible for some of the discrepancy in repeatability between the sagittal and transverse imaging methods but did not explain the discrepancy in repeatability between males and females. It was (unofficially) suspected that males would have poorer repeatability due to the higher proportion of lean upper body mass and increased noise as a result. However, having evaluated more than 20 statistical tests in this thesis at a significance level of $\alpha = 0.05$, it is possible that this finding was a false positive (type I error). Robustness was not evaluated in the transverse imaging method, however based on the

repeatability findings, it was suspected that the transverse method would not be robust to induced error. Recall that the robustness protocol investigated the ability to capture a misleading image; an image which appears acceptable but generates incorrect measurements. Such an error is expected to be more likely in the transverse method compared to the sagittal method due to the more diffuse echoes from deeper tissues and the additional anatomical targets present in the transverse method. For example, the transverse processes or the superior articular process of the inferior vertebral body could be misinterpreted and imaged by mistake.

The transverse imaging method compared well to surface-based optoelectronic motion capture measures in females across the three MMH tasks however a significant difference between the two methods was detected in males. This difference was not expected at the beginning of this study; however, it was observed that back musculature made imaging particularly difficult. While back musculature was not quantified by any precise means, it was noted by visual observation that males typically had larger erector spinae musculature which disrupted transverse imaging. It was also noted that the motion capture rigid bodies, originally placed over the L1 and T10 SPs, migrated over top of the erector spinae musculature upon axial rotation. In some cases, this had the effect of rotating the rigid body in the direction opposite to the actual observed motion. Both sources of error may have contributed to the differences observed between ultrasound and surface-based optoelectronic motion capture in males during the MMH tasks. These sources of error may also explain the discrepancies between the results of this thesis and the in-vitro results presented by McKinnon & Callaghan in 2019 which described extremely low error (a correlation >0.903 with motion capture). The issues of erector spinae bulk influencing both transducer and rigid body motion were not described in the previous in-vivo work of Mayberry (2017) since only passively held positions were tested in that investigation. The transverse method was also compared purely numerically to surface-based optoelectronic motion capture during the MMH tasks. The results indicated that at most four of 10 participants had sum-total ultrasound measurements within 2°

of surface-based optoelectronic motion capture. Part of the difficulty in accurately measuring lumbar axial rotation is the limited axial rotation ROM in the lumbar region (approximately 10°) (Fujii et al., 2007). A relatively small measurement error of just 1° amounts to 10% error when expressed relative to this small total measurement range.

The active, stiffened musculature and accompanying migration of rigid bodies was likely responsible for the less favourable axial rotation imaging performance shown in this thesis, but may improve with different transducer and rigid body geometries. As well, the transverse repeatability findings suggest that improvement would be obtained with controlled imaging duration, especially for female participants. Despite these apparent shortcomings, the transverse method added important measurement resolution to the MMH tasks and presents an approach that may help uncover important fundamental spine behaviour.

6.2.3 Acquisition Window

In the transverse imaging method, the tilting window was found to be 12.3° (4.4°) on average in the neutral and axially rotated positions. Theoretical measurements based on anatomical data fit to a 3D model were the basis for the hypothesized 20° window, however this value did not take imaging noise into consideration and therefore a smaller transverse imaging window was as expected. In the sagittal imaging method, the tilting window was 7.9° (4.94°) in the neutral position and 10.2° (5.23°) in the axially rotation position. These findings agreed with expectations based on previous in-vivo anatomical measurement but a difference in acquisition window between positions was not expected and cannot be logically explained at the moment.

6.3 Limitations

Both ultrasound measurement methods (sagittal and transverse) were previously validated separately in vivo by MRI. The goal of this study was to measure multiplanar motion using both methods

at the same time which allowed for simultaneous measurement of both lumbar flexion and axial rotation. While it may have been helpful to validate this study against MRI as well, this option was costly and resource intensive. Such a validation study may be pursued in the future.

Still, some limitations of this work should be considered. Sagittal plane imaging was suitable for less that 90th percentile height males (1.85m) and less than 99th percentile height females (1.85m). Beyond these percentiles, it was likely that the SPs of the participant would be too large to be reliably imaged due to the limited size of the ultrasound slice (44mm). During ultrasound imaging, surface-based optoelectronic motion capture was collected via rigid bodies placed at T10 and S1. Optoelectronic motion capture across the region of T10 to S1 could not be directly compared with the ultrasound measurements across the region of L1 to S1. This limitation was mitigated by adding an L1 rigid body after ultrasound imaging and the positions were quantified once again. Future uses of this methodology would also have to include these additional trials to enable direct comparison. Despite these limitations, this thesis successfully demonstrated the ability to measure multiplanar intervertebral kinematics, revealed outlier ROM, and movement sequencing during manual materials handling tasks.

6.4   Future Directions

Future research should investigate the use of automation and/or algorithms to process and analyze data more efficiently, and potentially in real-time. This modification would make the method more valuable in clinical or industrial settings where real time data would be a major advantage to both the patient and healthcare system by requiring fewer return appointments but may also to help the user to acquire higher quality data by providing immediate feedback during imaging. Additionally, intermediate peg-board positions should also be considered as they would help to eliminate extreme positions, thereby reducing the impact of muscle bulk on US measurement and surface-based motion capture rigid body migration, potentially improving transverse imaging performance. Lastly, small, and stretchable ultrasound devices which conform to the surface to which they are applied have been developed recently

(Guo et al., 2018). These devices are encouraging as it may be possible to attach a small transducer array over multiple spinal levels to track three-dimensional motion, potentially in real-time. For these methods to be applied immediately, different transducer geometries should be considered to mitigate the effects of the erector spine muscle bulk on transducer placement in the transverse orientation and possible consideration given to standardizing imaging time. Researchers should keep a keen eye on these devices as they develop as it will only improve the repeatability and robustness of these methods.

7 CONCLUSIONS

Previous research has explored the use of ultrasound in vitro and in-vivo, measuring single planar motion within passively held positions with high precision and accuracy. The goal of this thesis was to explore the use of ultrasound in measuring three-dimensional spine kinematics in vivo within actively held positions. Several error metrics were also defined and evaluated in order to ensure that the sagittal and transverse measurement methods could deliver acceptable results.

The sagittal imaging method (used for quantifying lumbar flexion) required one ultrasound image of two adjacent SPs. One point was digitized on each SP, generating a linear spacing measurement. This measurement could then be compared between different tasks in order to assess intervertebral motion in the sagittal plane. This method was shown to be robust and repeatable in the population studied and was able to uncover 14 instances of outlier ROM while surfaced-based optoelectronic motion capture identified only one throughout the same tasks. The transverse method (used for quantifying axial rotation) required an ultrasound image of just one vertebral body showing the spinous process and the laminae. The laminae were imaged perpendicular to the imaging direction so that the rotation of the ultrasound transducer mirrored the axial rotation of the vertebrae. The accuracy and repeatability of this method may improve with improvements in ultrasound technology. Nonetheless, this thesis demonstrated that it is possible to measure multiplanar intervertebral motion via US. This improved resolution may help to identify riskier movement sequences which may appear normal in a surface-based motion capture investigation.

8   REFERENCES

Adams, M.A., 1995. Mechanical testing of the spine, an appraisal results, and conclusions. *Spine*. 20, 2151–2156.

Ang, C., Nairn, B.C., Schinkel-Ivy, A., Drake, J.D.M., 2016. Seated maximum flexion: An alternative to standing maximum flexion for determining presence of flexion-relaxation? *J. Back Musculoskelet. Rehabil.* 29, 249–258.

Aylott, C.E.W., Puna, R., Robertson, P.A., Walker, C., 2012. Spinous process morphology: The effect of ageing through adulthood on spinous process size and relationship to sagittal alignment. *Eur. Spine J.* 21, 1007–1012.

Bartlett, J.W., Frost, C., 2008. Reliability, repeatability and reproducibility: analysis of measurement errors in continuous variables. *Ultrasound Obstet. Gynecol*. 31, 466–475.

Benoit, D.L., Ramsey, D.K., Lamontagne, M., Xu, L., Wretenberg, P., Renström, P., 2006. Effect of skin movement artifact on knee kinematics during gait and cutting motions measured in vivo. *Gait Posture* 24, 152–164.

BIPM, 2008. Evaluation of measurement data — Guide to the expression of uncertainty in measurement. *Bur. Int. des Poids Mes*. 35.

Callaghan, J.P., McGill, S.M., 2001. Intervertebral disc herniation: Studies on a porcine model exposed to highly repetitive flexion/extension motion with compressive force. *Clin. Biomech*. 16, 28–37.

Cappozzo, A., Catani, F., Leardini, A., Benedetti, M.G., Della Croce, U., 1996. Position and orientation in space of bones during movement: experimental artefacts. *Clin. Biomech*. 11, 90–100.

Chleboun, G.S., Amway, M.J., Hill, J.G., Root, K.J., Murray, H.C., Sergeev, A. V., 2012. Measurement of segmental lumbar spine flexion and extension using ultrasound imaging. *J. Orthop. Sport. Phys. Ther.* 42, 880–885.

Cholewicki, J., McGill, S.M., 1992. Lumbar posterior ligament involvement during extremely heavy lifts estimated from fluoroscopic measurements. *J. Biomech*. 25, 17–28.

Drake, J.D.M., Callaghan, J.P., 2008. Do flexion/extension postures affect the in vivo passive lumbar spine response to applied axial twist moments? *Clin. Biomech*. 23, 510–519.

Drake, J.D.M., Dobson, H., Callaghan, J.P., 2008. The influence of posture and loading on interfacet spacing: An investigation using magnetic resonance imaging on porcine spinal units. *Spine*. 33, 728–734.

Drake, J.D.M., Fischer, S.L., Brown, S.H.M., Callaghan, J.P., 2006. Do exercise balls provide a training advantage for trunk extensor exercises? A biomechanical evaluation. *J. Manipulative Physiol. Ther*. 29, 354–362.

Drake, J.D.M., Aultman, C.D., McGill, S.M., Callaghan, J.P., 2005. The influence of static axial torque in combined loading on intervertebral joint failure mechanics using a porcine model. *Clin. Biomech*. 20, 1038–1045.

Fazey, P.J., Song, S., Mønsås, Å., Johansson, L., Haukalid, T., Price, R.I., Singer, K.P., 2006. An MRI investigation of intervertebral disc deformation in response to torsion. *Clin. Biomech*. 21, 538–542.

Frigo, C., Carabalona, R., Dalla Mura, M., Negrini, S., 2003. The upper body segmental movements during walking by young females. *Clin. Biomech*. 18, 419–425.

Gatton, M.L., Pearcy, M.J., 1999. Kinematics and movement sequencing during flexion of the lumbar spine. *Clin. Biomech*. 14, 376–383.

Gregersen, G., Lucas, D., 1967. An in vivo study of the axial rotation of the human thoracolumbar spine. *J. Bone Jt. Surg.* 49-A, 247–262.

Gregory, D.E., Callaghan, J.P., 2008. Prolonged standing as a precursor for the development of low back discomfort: An investigation of possible mechanisms. *Gait Posture* 28, 86–92.

Guo, Yue, T., Wenbo, Z., Yang, L., Akihiro, N., Simone, S., Qifa, Z., Matt, P., Francesco Lanza di, S., Sheng Xu, H.H., Xuan, Z., Chonghe, W., Lin, Z., Xiaoshi, L., Seunghyun, L., Zhenlong, H., Ruimin, C., Zeyu, C., Chunfeng, W., Yue, G., Yimu, C., Yusheng, L., Tianjiao, Z., NamHeon, K., Yuxuan, 2018. Stretchable ultrasonic transducer arrays for three-dimensional imaging on complex surfaces. *Sci. Adv*. 1–12.

Hodgson, R., O'Connor, P.J., Grainger, A.J., 2012. Tendon and ligament imaging. *Br. J. Radiol*. 85, 1157–1172.

Katz, J.N., 2006. Lumbar disc disorders and low-back pain: socioeconomic factors and consequences. *J. Bone Joint Surg. Am.* 88-A, 21–24.

Kawchuk, G.N., Prasad, N., Parent, E., Chapman, S., Custodio, M., Manzon, M., Wiebe, A., Dhillon, S., 2011.Spinal landmark depth in relation to body mass index. *Man. Ther.* 16, 384–387.

Koo, T.K., Li, M.Y., 2016. A Guideline of Selecting and Reporting Intraclass Correlation Coefficients for Reliability Research. *J. Chiropr. Med*. 15, 155–163.

Lumsden, R., Morris, J., 1968. An in vivo study of axial rotation and immobilization at the lumbosacral joint. *J. Bone Jt. Surg*. 50-A, 1591–1602.

Lund, T., Nydegger, T., Schlenzka, D., Oxland, T.R., 2002. Three-dimensional motion patterns during active bending in patients with chronic low back pain. *Spine*. 27, 1865–1874.

Lundgren, P., Nester, C., Liu, A., Arndt, A., Jones, R., Stacoff, A., Wolf, P., Lundberg, A., 2008. Invasive in vivo measurement of rear-, mid- and forefoot motion during walking. *Gait Posture* 28, 93–100.

Mayberry, G., 2017. Validating the use of ultrasound to measure lumbar vertebral twist, in: American Society for Biomechanics Annual Conference. Boulder, CO.

Mayberry, G., 2015. Understanding axial rotation in the lumbar spine and its effects on associated nerve tissue. York University. MSc Thesis, 50-58.

McGill, S., Andersen, J., Cannon, J., 2015. Muscle activity and spine load during anterior chain whole body linkage exercises: the body saw, hanging leg raise and walkout from a push-up. *J. Sports Sci*. 33, 419–426.

McKinnon, C.D., Callaghan, J.P., 2019. Validation of an ultrasound protocol to measure intervertebral axial twist during functional twisting movements in isolated functional spinal units. 45, 642–649.

Nairn, B.C., 2017. From structure to function: a characterization of the upper thoracic spine. York University. PhD Thesis, 45-49.

Nester, C., Jones, R.K., Liu, A., Howard, D., Lundberg, A., Arndt, A., Lundgren, P., Stacoff, A., Wolf, P., 2007. Foot kinematics during walking measured using bone and surface mounted markers. *J. Biomech*. 40, 3412–3423.

Ochia, R.S., Inoue, N., Renner, S.M., Lorenz, E.P., Lim, T.H., Andersson, G.B.J., An, H.S., 2006. Three-dimensional in vivo measurement of lumbar spine segmental motion. *Spine*. 31, 2073–2078.

Panjabi, M.M., Goel, V.K., Takata, K., 1982. Physiologic strains in the lumbar spinal ligaments. An in vitro biomechanical study. *Spine*. 7, 192–203.

Panjabi, M.M., Goel, V., Oxland, T., Takata, K., Duranceau, J., Krag, M., Price, M., 1991. Human lumbar vertebrae quantitative three-dimensional anatomy. *Spine*. 17, 299–306.

Pearcy, M.J., Tibrewal, S.B., 1984. Axial rotation and lateral bending in the normal lumbar spine measured by three-dimensional radiography. *Spine*. 9, 582–587.

Pearcy, M.J., Portek, I., Shepherd, J., 1984. Three-dimensional x-ray analysis of normal movement in the lumbar spine. *Spine*. 9, 294–297.

Reinschmidt, C., Bogert, A. Van Den, 1997. Effect of skin movement on the analysis of skeletal knee joint motion during running. *J. Biomech*. 30, 729–732.

Rozumalski, A., Schwartz, M.H., Wervey, R., Swanson, A., Dykes, D.C., Novacheck, T., 2008. The in vivo three-dimensional motion of the human lumbar spine during gait. *Gait Posture* 28, 378–384.

Sahni, I.K., Hipp, J.A., Kirking, B.C., Alexander, J.W., Esses, S.I., 1999. Use of percutaneous transpedicular external fixation pins to measure intervertebral motion. *Spine*. 1890-1893.

Schinkel-Ivy, A., DiMonte, S., Drake, J.D.M., 2015. Repeatability of kinematic and electromyographical measures during standing and trunk motion: How many trials are sufficient? *J. Electromyogr. Kinesiol.* 25, 232–238.

Schinkel-Ivy, A., Pardisnia, S., Drake, J.D.M., 2014. Head and arm positions that elicit maximal voluntary trunk range-of-motion measures. *J. Appl. Biomech*. 30, 689–696.

Stinton, S.K., 2011. Development, validation, and application of a noninvasive spinal motion measurement system. University of Kentucky. 17.

Suzuki, S., Yamamuro, T., Shikata, J., Shimizu, K., Hirokazu, I., 1989. Ultrasound measurement of vertebral rotation in idiopathic scoliosis. *J. Bone Jt. Surg*. 252-255

van den Hoorn, W., Coppieters, M.W., van Dieën, J.H., Hodges, P.W., 2016. Development and validation of a method to measure lumbosacral motion using ultrasound imaging. *Ultrasound Med. Biol.* 42, 1221–1229.

Vos, T., Abajobir, A.A., Abbafati, C., Abbas, K.M., Abate, K.H., Abd-Allah, F., 2017. Global, regional, and national incidence, prevalence, and years lived with disability for 328 diseases and injuries for 195 countries, 1990-2016: A systematic analysis for the Global Burden of Disease Study 2016. *Lancet* 390, 1211–1259.

Westblad, P., Hashimoto, T., Winson, I., Lundberg, A., Arndt, A., 2002. Differences in ankle-joint complex motion during the stance phase of walking as measured by superficial and bone-anchored markers. *Foot Ankle Int.* 23, 856–863.

White, A.A., Panjabi, M.M., 1978. The basic kinematics of the human spine. A review of past and current knowledge. *Spine*. 12-20.

Yamamoto, I., Panjabi, M., Crisco, T., Oxland, T., 1989. Three-dimensional movements of the whole lumbar spine and lumbosacral joint. *Spine*. 14, 1256–1260.

9 APPENDIX A – ERROR AND REPEATABILITY PROTOCOLS
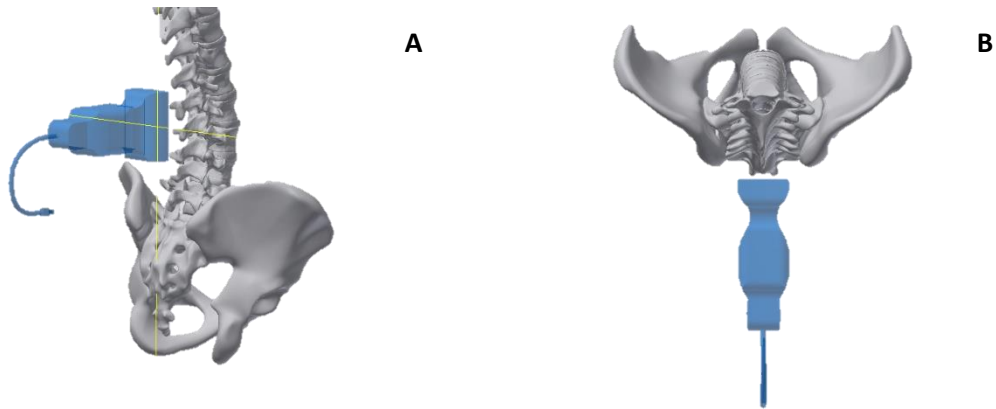
Figure 9.1 - A: Posterolateral view showing the sagittal imaging configuration. Ultrasound transducer centred over L1-L2. B: Transverse plane view looking superior to inferior.
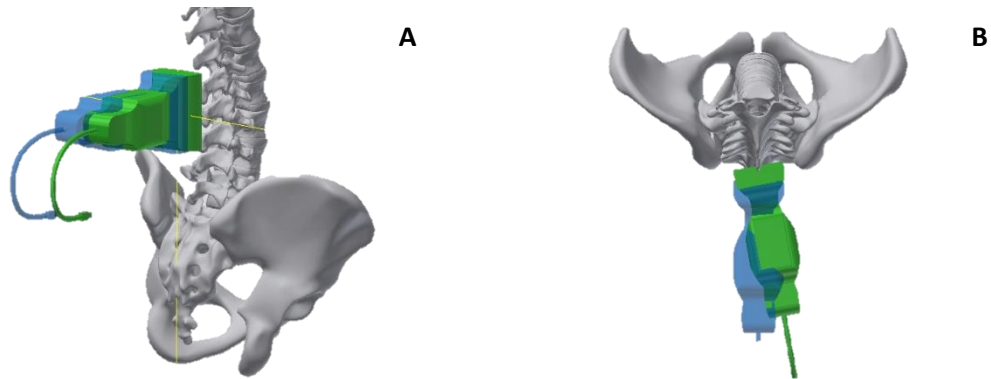
Figure 9.2 - A: Posterolateral view showing the ideal (blue) and tilted (green) sagittal plane imaging configuration. B: Transverse plane view looking inferiorly of the same. When performed in both directions, this generates the tilting acquisition window about the longitudinal axis for the sagittal orientation.
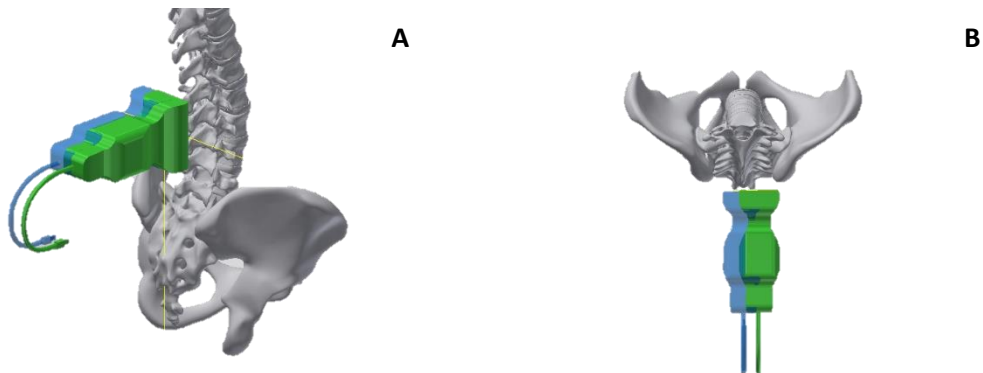
Figure 9.3 - A: Posterolateral view showing the ideal (blue) and translated (green) sagittal plane imaging configuration. B: Transverse plane view looking inferiorly of the same. When performed in both directions, this generates the translation acquisition window along the medio-lateral axis for the sagittal orientation.
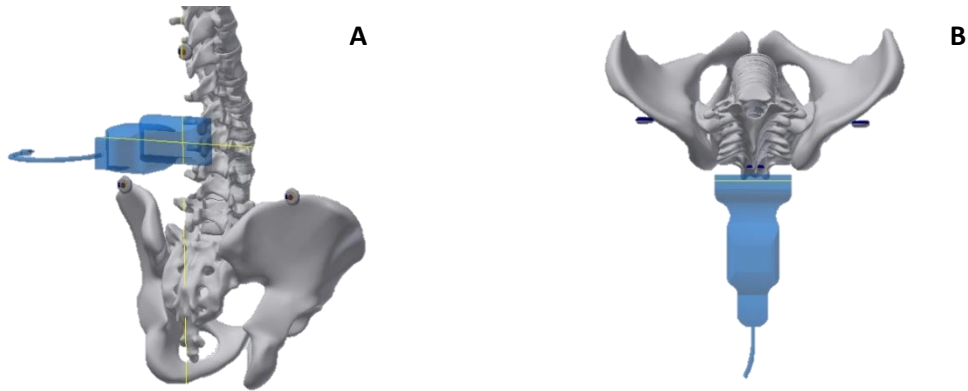
Figure 9.4 - A: Posterolateral view showing the transverse imaging configuration. Ultrasound transducer centred over L1-L2. B: Transverse plane view looking inferiorly of the same.
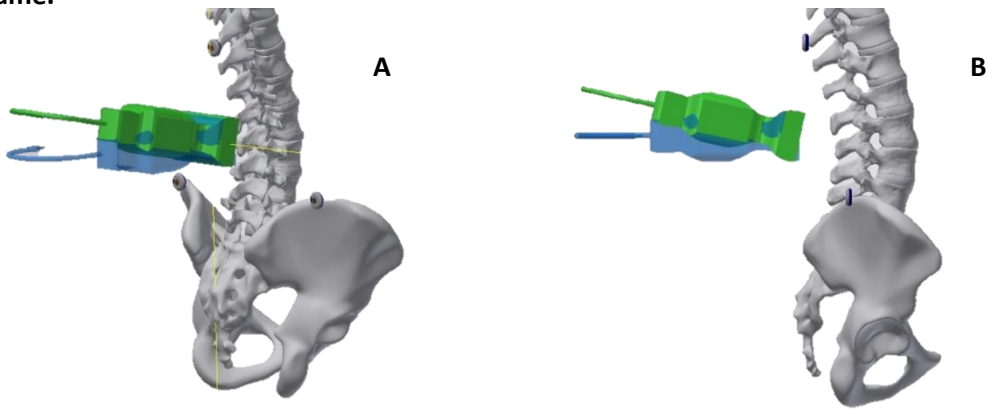
Figure 9.5 - A: Posterolateral view showing the ideal (blue) and tilted (green) transverse plane imaging configuration. B: Sagittal plane view of the same. When performed in both directions, this generates the tilting acquisition window about the medio-lateral axis for the transverse orientation.
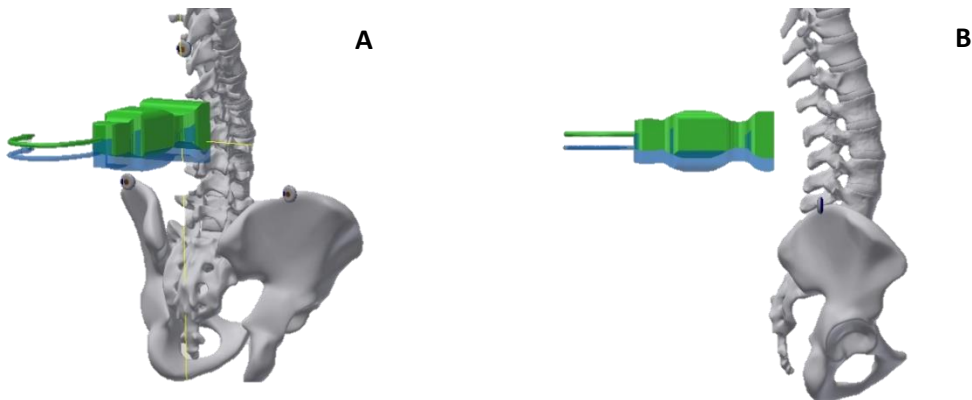
Figure 9.6 - A: Posterolateral view showing the ideal (blue) and tilted (green) transverse plane imaging configuration. B: Sagittal view of the same. When performed in both directions, this generates the translating acquisition window along the longitudinal axis for the transverse orientation.

10 APPENDIX B – DETAILED PROTOCOL

| ASSESSING THE USE OF ULTRASOUND TO QUANTIFY SPINE KINEMATICS				DATA OUTPUT		
				MOCAP	US	VID
GENERAL PREPARATION						
1			Informed consent and activity questionnaires (IPAQ and custom health questionnaire) will be completed. Anthropometric measures (e.g. weight, height, age, sex, body composition) will be taken.			X
2			Participants will have their spine palpated and/or imaged with ultrasound to identify landmarks. Landmarks will be indicated with marker 4" away from midline.			X
3			Plug cube into channel 1. Turn on cameras and System Control Unit (SCU). Start up NDI First Principles.			X
4			Register space. Define coordinate system.			X
5			Rigid bodies are placed on participant at S1, T11 and C7.			X
6			Plug Smart Markers / tools into SCU.			X
	a		Channel 1 of SCU: rigid bodies. S1 into line 1 of strober, T11 into line 2 of strober, C7 into line 3 of strober.			X
	b		Channel 2 of SCU: ultrasound transducer rigid body. Connect rigid body to ultrasound transducer. Plug wire into line 1 of strober.			X
	c		Channel 3 of SCU: digitizing pen. Plug wire into line 1 of strober.			X
7			In NDI First Principles, start new experiment.			X
8			Ensure number of SMART MARKERs shows as 21. Configure rigid bodies and digitized points.			X
	a		SMART MARKERs 1-6: S1_6MARKER.rig (for tracking)			X
		i	Digitized Point 1: "L_ASIS" (for modeling)			X
		ii	Digitized Point 2: "R_ASIS" (for modeling)			X
		iii	Digitized Point 3: "L_PSIS" (for modeling)			X
		iv	Digitized Point 4: "R_PSIS" (for modeling)			X
	b		SMART MARKERs 7-12: T12_6MARKER.rig (note: this SMART MARKER is placed at T11 – for tracking)			X
	c		SMART MARKERs 13-18: C7_6MARKER.rig (for tracking)			X
		i	Digitized Point 1: "L_SCAP" (inferior angle of left scapula – for modeling)			X
		ii	Digitized Point 2: "R_SCAP" (for modeling)			X
	d		SMART MARKERs 19-21: TRANSD.rig (for tracking)			X
		i	Digitized Point 1: "TRANSD_1" (medial-cranial point on transducer face)			X

		ii		Digitized Point 2: "TRANSD_2" (medial-caudal point on transducer face)				X
		iii		Digitized Point 3: "TRANSD_3" (lateral-caudal point on transducer face)				X
		iv		Digitized Point 4: "TRANSD_4" (lateral-cranial point on transducer face)				X
9			With participant standing, digitize points on participant.			X
10			After digitizing, in First Principles view points in spatial view – ensure rigids are green. View points in spatial view – ensure point clusters are in realistic positions.			X
11			Neutral sagittal reference imaging			
	a		Ideal sagittal image is taken at L1-L2		X	X
	b		Ideal sagittal image is taken at L2-L3		X	X
	c		Ideal sagittal image is taken at L3-L4	X	X	X
	d		Ideal sagittal image is taken at L4-L5		X	X
	e		Ideal sagittal image is taken at L5-S1		X	X
11			Neutral transverse reference imaging			
	a		Ideal transverse image is taken at L1	X	X	
	b		Ideal sagittal image is taken at L2	X	X	
	c		Ideal sagittal image is taken at L3	X	X	
	d		Ideal sagittal image is taken at L4	X	X	
	e		Ideal sagittal image is taken at L5	X	X	
12			Full flexion reference imaging			
	a		Ideal sagittal image is taken at L1-L2		X	X
	b		Ideal sagittal image is taken at L2-L3		X	X
	c		Ideal sagittal image is taken at L3-L4	X	X	X
	d		Ideal sagittal image is taken at L4-L5		X	X
			Ideal sagittal image is taken at L5-S1		X	X

NEUTRAL ERROR IMAGING

13			Participant lays face-down on padded table in a neutral-spine posture. Head in cradle, hands at side.			X
14			Sagittal transducer orientation images at **L1-L2**			X
	a		Ideal image is located. Image is labeled on US device.			X
	b		Ultrasound loop (m-mode) and mocap begin in synch.			X
	c		Transducer is rotated **towards** researcher (left) until image is lost. Loop ends in synch with mocap.	X	X	X

	d		Ideal image is relocated. Image is labeled on US device.			X
	e		Ultrasound loop (m-mode) and mocap begin in synch.	X	X	X
	f		Transducer is rotated **away** (right) from researcher until image is lost. Loop ends in synch with mocap.			X
	g		Ideal image is relocated. Image is labeled on US device.			X
	h		Ultrasound loop (m-mode) and mocap begin in synch.	X	X	X
	i		Transducer is translated **towards** (left) researcher until image is lost. Loop ends in synch with mocap.			X
	j		Ideal image is relocated. Image is labeled on US device.			X
	k		Ultrasound loop (m-mode) and mocap begin in synch.	X	X	X
	l		Transducer is translated **away (**right) from researcher until image is lost. Loop ends in synch with mocap.			X
15			Transverse transducer orientation images at **L1**			X
	a		Ideal image is located. Image is labeled on US device.			X
	b		Ultrasound loop (m-mode) and mocap begin in synch.	X	X	X
	c		Transducer is rotated **towards** (caudally) researcher until image is lost. Loop ends in synch with mocap.			X
	d		Ideal image is relocated. Image is labeled on US device.			X
	e		Ultrasound loop (m-mode) and mocap begin in synch.	X	X	X
	f		Transducer is rotated **away** (cranially) from researcher until image is lost. Loop ends in synch with mocap.			X
	g		Ideal image is relocated. Image is labeled on US device.			X
	h		Ultrasound loop (m-mode) and mocap begin in synch.	X	X	X
	i		Transducer is translated **towards** (caudally) researcher until image is lost. Loop ends in synch with mocap.			X
	j		Ideal image is relocated. Image is labeled on US device.			X
	k		Ultrasound loop (m-mode) and mocap begin in synch.	X	X	X
	l		Transducer is translated **away** (cranially) from researcher until image is lost. Loop ends in synch with mocap.			X
FLEXION ERROR IMAGING						
16			With participant remaining face-down, a BOSU Ball is located beneath the abdomen to induce supported lumbar flexion.			X
17			Sagittal transducer orientation images at **L1-L2**			X
	a		Ideal image is located. Image is labeled on US device.			X
	b		Ultrasound loop (m-mode) and mocap begin in synch.	X	X	X
	c		Transducer is rotated **towards** researcher (left) until image is lost. Loop ends in synch with mocap.			X
	d		Ideal image is relocated. Image is labeled on US device.			X

	e		Ultrasound loop (m-mode) and mocap begin in synch.	X	X	X
	f		Transducer is rotated **away** (right) from researcher until image is lost. Loop ends in synch with mocap.			X
	g		Ideal image is relocated. Image is labeled on US device.			X
	h		Ultrasound loop (m-mode) and mocap begin in synch.	X	X	X
	i		Transducer is translated **towards** (left) researcher until image is lost. Loop ends in synch with mocap.			X
	j		Ideal image is relocated. Image is labeled on US device.			X
	k		Ultrasound loop (m-mode) and mocap begin in synch.	X	X	X
	l		Transducer is translated **away (**right) from researcher until image is lost. Loop ends in synch with mocap.			X
ROTATION ERROR IMAGING						
18			Participant bends their right knee and hip to 90°, or as far as possible, dictated by comfort. Foam is used between the knees, and straps are used to maintain the position of the shoulders, knees and hips.			X
19			Transverse transducer orientation images at **L1**			X
	a		Ideal image is located. Image is labeled on US device.			X
	b		Ultrasound loop (m-mode) and mocap begin in synch.	X	X	X
	c		Transducer is rotated **towards** (caudally) researcher until image is lost. Loop ends in synch with mocap.			X
	d		Ideal image is relocated. Image is labeled on US device.			X
	e		Ultrasound loop (m-mode) and mocap begin in synch.	X	X	X
	f		Transducer is rotated **away** (cranially) from researcher until image is lost. Loop ends in synch with mocap.			X
	g		Ideal image is relocated. Image is labeled on US device.			X
	h		Ultrasound loop (m-mode) and mocap begin in synch.	X	X	X
	i		Transducer is translated **towards** (caudally) researcher until image is lost. Loop ends in synch with mocap.			X
	j		Ideal image is relocated. Image is labeled on US device.			X
	k		Ultrasound loop (m-mode) and mocap begin in synch.	X	X	X
	l		Transducer is translated **away** (cranially) from researcher until image is lost. Loop ends in synch with mocap.			X
SIMILATED MMH IMAGING						
20			Participant is briefed on MMH task requirements.			X
21			Pelvis of participant is fixed to table at the height of the illia with ratchet straps. A foam pad is located between the table and the participant for comfort. Dominant shoulder is lined up with the holes on the side of the dominant arm.			X
22			Participant moves dowel with dominant hand to position 1 (pure rotation)			X
	a		Ideal sagittal image is taken at **L1-L2**	X	X	X

	b		Ideal sagittal image is taken at **L2-L3**	X	X	X
	c		Ideal sagittal image is taken at **L3-L4**	X	X	X
	d		Ideal sagittal image is taken at **L4-L5**	X	X	X
	e		Ideal sagittal image is taken at **L5-S1**	X	X	X
	f		Ideal transverse image is taken at **L1**	X	X	X
	g		Ideal transverse image is taken at **L2**	X	X	X
	h		Ideal transverse image is taken at **L3**	X	X	X
	i		Ideal transverse image is taken at **L4**	X	X	X
	j		Ideal transverse image is taken at **L5**	X	X	X
23			Participant moves dowel to position 2 (rotation + flexion)			X
	a		Ideal sagittal image is taken at **L1-L2**	X	X	X
	b		Ideal sagittal image is taken at **L2-L3**	X	X	X
	c		Ideal sagittal image is taken at **L3-L4**	X	X	X
	d		Ideal sagittal image is taken at **L4-L5**	X	X	X
	e		Ideal sagittal image is taken at **L5-S1**	X	X	X
	f		Ideal transverse image is taken at **L1**	X	X	X
	g		Ideal transverse image is taken at **L2**	X	X	X
	h		Ideal transverse image is taken at **L3**	X	X	X
	i		Ideal transverse image is taken at **L4**	X	X	X
	j		Ideal transverse image is taken at **L5**	X	X	X
24			Participant moves dowel to position 3 (pure flexion)			X
	a		Ideal sagittal image is taken at **L1-L2**	X	X	X
	b		Ideal sagittal image is taken at **L2-L3**	X	X	X
	c		Ideal sagittal image is taken at **L3-L4**	X	X	X
	d		Ideal sagittal image is taken at **L4-L5**	X	X	X
	e		Ideal sagittal image is taken at **L5-S1**	X	X	X
	f		Ideal transverse image is taken at **L1**	X	X	X
	g		Ideal transverse image is taken at **L2**	X	X	X
	h		Ideal transverse image is taken at **L3**	X	X	X
	i		Ideal transverse image is taken at **L4**	X	X	X

	j		Ideal transverse image is taken at **L5**	X	X	X
25			The ultrasound gel is cleaned with tissue, and the probe is cleaned and disinfected. The motion capture SMART MARKERs are removed.			
26			Participants complete an exit survey consisting of five questions on their experience in the study, including whether they felt the imaging during the manual materials handling impacted how they moved.			